MSc thesis May 2026

Arctic Instantaneous Clear-sky Radiative Forcing Research under Different Vertical Structures of Greenhouse Gases

Jiayi Qin

UNIVERSITY OF HELSINKI

Arctic Instantaneous Clear-sky Radiative Forcing Research under Different Vertical Structures of Greenhouse Gases

Jiayi Qin

30 ECTS thesis approved in partial fulfilment of a double Master degree in Atmospheric Sciences, from Nanjing University and University of Helsinki.

Academic supervisors:

Prof. Jianning Sun, Prof. Huilin Chen

Academic examiners:

Prof. Ivan Mammarella

University of Helsinki

Nanjing University

Nanjing, May 2026

学校代码：10284

分 类 号：P422.2

密　　级：公开

U　D　C：551.5

学　　号：502024380020

南京大学

硕 士 学 位 论 文

论 文 题 目	温 室 气 体 不 同 垂 直 结 构 下 的 北 极 晴 空 瞬 时 辐 射 强 迫 研 究
作 者 姓 名	秦 佳 怡
专 业 名 称	大 气 科 学
研 究 方 向	温 室 气 体 辐 射 强 迫
导 师 姓 名	孙 鉴 泞 教 授 、 陈 辉 林 教 授

2026 年 5 月 20 日

答辩委员会主席 朱 延 年

评　　阅　　人 汤 帅 奇

董 新 奕

朱 延 年

Ivan Mammarella

论 文 答 辩 日 期　2026 年 5 月 13 日

研究生签名：

导 师 签 名：

Nanjing University

Master's Dissertation

Arctic Instantaneous Clear-sky Radiative Forcing Research under Different Vertical Structures of Greenhouse Gases

By Jiayi Qin

Major：Atmospheric Science

Advisor：Prof. Jianning Sun, Prof. Huilin Chen

Nanjing-Helsinki Institute in Atmospheric and Earth System Sciences, Nanjing University

June，2026

南京大学研究生毕业论文中文摘要首页用纸

毕业论文题目： 温室气体不同垂直结构下的北极晴空瞬时辐射强迫研究

大气科学 专业 2024 级硕士生姓名： 秦佳怡

指导教师（姓名、职称）： 孙鉴泞教授、陈辉林教授

摘 要

自工业革命以来，主要以二氧化碳（CO_2）和甲烷（CH_4）为代表的长寿命温室气体持续增加，显著增强了地球系统的正辐射强迫。现有辐射强迫估算多基于柱平均浓度并假设气体垂直充分混合，忽略了实际大气中显著存在的垂直非均匀结构。北极地区由于气溶胶浓度低、层结稳定、平流层逆温显著及水汽含量偏低，其辐射过程对温室气体垂直分布更加敏感。本文针对“温室气体垂直结构如何调制北极瞬时晴空长波辐射强迫”这一核心问题，系统评估 CO_2 与 CH_4 垂直分布非均匀性对辐射收支及加热率结构的影响，并分析其空间代表性及碳中和情景下的响应特征。

本研究选取芬兰北部 Sodankylä站点 2017 年 4 –10 月 10 次 AirCore 高分辨率温室气体廓线数据，结合 RRTMG 模型，构建“观测垂直廓线”与“柱平均均匀分布”对比实验，将温室气体均匀分布的净长波辐射通量值减去观测垂直廓线分布的净长波辐射通量值定义为由垂直结构引起的逐层辐射强迫响应（ΔRF），并进一步计算 TOA 辐射强迫响应（ΔRF_{TOA}）。在此基础上，引入层辐射敏感度核方法识别关键敏感层，并基于 SD-WACCM 背景场在不同空间尺度下评估单站结果的区域代表性；同时，在 SSP1-2.6 情景下构建未来背景场，分析垂直结构效应的变化。结果表明：

（1）CO_2 辐射强迫响应呈“低层正、高层负”结构。这种垂直结构的强度存在明显季节差异：春季ΔRF_{TOA} 为-0.08 ~ -0.11 W m^{-2}，显著强于秋季（-0.01 ~

-0.04 W m^{-2}）；而 CH_4 在对流层中下部产生约 0.02 ~ 0.03 W m^{-2} 的正强迫，高层转为弱负值。其ΔRF_{TOA}主要处于-0.01 ~ -0.03W m^{-2} 左右，春季略低于秋季。

（2）层敏感性分析显示，CO_2 关键敏感层位于 700–200 hPa，敏感度核的最大值约 8×10^{-4} ~ 1×10^{-3} W m^{-2} ppm^{-1}，CH_4 关键敏感层位于 900–400 hPa，敏感度核的最大值约 3×10^{-3} ~ 5×10^{-3} W m^{-2} ppm^{-1}，表明辐射效应具有显著高度依赖性。

（3）空间代表性分析表明，当背景场由 Sodankylä 地区单点扩展至其周边 ±2.5 ° 区域平均及北极圈平均时，CO_2 逐层辐射强迫响应对空间尺度不敏感（最大差异约 0.006 W m^{-2}）；相比之下，CH_4 逐层辐射强迫响应在北极圈平均背景下略有减弱（对流层差异约 0.01 W m^{-2}），但垂直结构基本保持一致。

（4）在 SSP1-2.6 情景下，尽管 CO_2 增加约 50 ppm、CH_4 减少约 700 ppb，两者ΔRF_{TOA}均由负转正。这表明ΔRF_{TOA}的变化主要受背景大气状态变化的调制，其中水汽增加与温度结构调整共同影响辐射强迫响应。

尽管本文基于晴空瞬时条件，未考虑云辐射效应与快速调整过程，且未来情景中假设垂直结构形态不变，但结果表明：当前北极地区若使用温室气体均匀分布廓线将低估向外长波辐射通量；而在未来碳中和情景下则可能高估向外长波辐射通量。上述结论为改进极地辐射通量估算方法、优化气候模式中温室气体垂直参数化方案以及深化对北极放大辐射机制的理解提供了新的依据。

关键词：辐射强迫；垂直剖面；温室气体；RRTMG；北极

南京大学研究生毕业论文英文摘要首页用纸

THESIS： Arctic Instantaneous Clear-sky Radiative Forcing Research under Different Vertical Structures of Greenhouse Gases

SPECIALIZATION: Atmospheric Science

POSTGRADUATE: Jiayi Qin

MENTOR: Professor Jianning Sun, Professor Huilin Chen

Abstract

Since the Industrial Revolution, long-lived greenhouse gases mainly represented by carbon dioxide (CO_2) and methane (CH_4) have continuously increased, significantly enhancing the positive radiative forcing of the Earth system. Existing estimates of radiative forcing are mostly based on column-mean concentrations and assume that gases are vertically well mixed, thereby neglecting the pronounced vertical inhomogeneity in the real atmosphere. In the Arctic, due to low aerosol concentrations, stable stratification, strong stratospheric temperature inversion, and low water vapor content, radiative processes are more sensitive to the vertical distribution of greenhouse gases. Against this background, this study focuses on the key scientific question of how the vertical structure of greenhouse gases modulates instantaneous clear-sky longwave radiative forcing in the Arctic. The effects of vertical inhomogeneity of CO_2 and CH_4 on radiative fluxes and heating rate structures are systematically quantified, and their spatial representativeness and responses under a carbon neutrality scenario are further investigated.

This study is based on 10 AirCore high-resolution vertical profiles of greenhouse gases observed at the Sodankylä site in northern Finland from April to October 2017. Using the Rapid Radiative Transfer Model for GCMs (RRTMG), two scenarios are

constructed: the ‘observed vertical profile’ and the ‘column-mean uniform distribution.’ The layer-resolved radiative forcing response (ΔRF) induced by vertical structure is defined as the net longwave radiative flux under the uniform distribution minus that under the observed vertical profile. And the corresponding radiative forcing response at the top of the atmosphere (ΔRF_{TOA}) is further calculated. On this basis, a layer radiative sensitivity kernel method is introduced to identify key sensitive layers. In addition, spatial representativeness is evaluated using SD-WACCM background fields at different spatial scales, and future changes in radiative forcing responses to vertical structure effects are analyzed under the SSP1-2.6 scenario. The results show that:

(1) The radiative forcing response of CO_2 shows a typical “positive in the lower layers and negative in the upper layers” structure. The strength of this vertical structure exhibits significant seasonal differences: the ΔRF_{TOA} in spring ranges from -0.08 to -0.11 W m^{-2}, significantly stronger than that in autumn (-0.01 to -0.04 W m^{-2}). CH_4 produces a positive radiative forcing of about 0.02 to 0.03 W m^{-2} in the lower to middle troposphere, while it turns into a weak negative value in the upper layers. The ΔRF_{TOA} mainly ranges from -0.01 to -0.03 W m^{-2}, with slightly lower values in spring than in autumn.

(2) The layer sensitivity analysis indicates that the key sensitive layer for CO_2 is located in the mid–upper troposphere (700–200 hPa), with a max sensitivity kernel of about 8×10^{-4} ~ 1×10^{-3} W m^{-2} ppm^{-1}, while the key sensitive layer for CH_4 is located in the lower–middle troposphere (900–400 hPa), with a max sensitivity kernel of about 3×10^{-3} ~ 5×10^{-3} W m^{-2} ppm^{-1}, demonstrating a strong altitude dependence of radiative effects.

(3) Spatial representativeness analysis shows that when the background field is extended from the single grid at Sodankylä to the surrounding $\pm 2.5^\circ$ regional average and further to the Arctic-wide average, the layer-resolved radiative forcing of CO_2 is insensitive to spatial scale (maximum difference ~0.006 W m^{-2}). In contrast, CH_4 exhibits a slight overall reduction under Arctic-mean background conditions (difference ~0.01 W m^{-2} in the troposphere), while its vertical structure remains

generally consistent.

(4) Under the SSP1-2.6 scenario, despite an increase of about 50 ppm in CO_2 and a decrease of about 700 ppb in CH_4, both exhibit a transition of ΔRF_{TOA} from negative to positive values. This indicates that the variation in ΔRF_{TOA} is primarily modulated by changes in the background atmospheric state, in which increases in water vapor and adjustments in the temperature structure jointly influence the radiative forcing response.

Although this study is conducted under instantaneous clear-sky conditions and does not account for cloud radiative effects or rapid atmospheric adjustments, and assumes unchanged vertical distribution shapes in future scenarios, the results indicate that using a uniform greenhouse gas profile in the present Arctic leads to an underestimation of outgoing longwave radiation. In contrast, under future carbon neutrality conditions, it may overestimate the outgoing longwave radiation. These findings provide new insights for improving radiative flux estimates in polar regions, optimizing vertical parameterizations of greenhouse gases in climate models, and advancing the understanding of Arctic amplification mechanisms.

Keywords: Radiative forcing; Vertical profiling; Greenhouse gases; RRTMG; Arctic

Contents

1 Introduction

1.1 Research background and significance

Since the Industrial Revolution, human activities have led to a continuous increase in atmospheric greenhouse gas concentrations, significantly altering the Earth's energy balance. Long-lived greenhouse gases represented by CO_2 and CH_4 have shown a persistent upward trend over the past century, and their radiative effects have become the primary drivers of global warming. Extensive observational evidence and climate model simulations indicate that increasing greenhouse gas concentrations enhance the absorption of longwave radiation within the atmosphere and reduce the net outgoing longwave radiation to space, thereby generating positive radiative forcing and increasing global mean temperature.

Radiative forcing can be categorized into instantaneous radiative forcing, adjusted radiative forcing, and effective radiative forcing according to different definitions. Among these, instantaneous clear-sky radiative forcing refers to the change in net radiative flux at the top of the atmosphere caused directly by variations in atmospheric composition, without considering clouds or rapid atmospheric adjustment processes[1]. It provides a direct measure of the pure radiative effects of greenhouse gases and is particularly suitable for isolating the physical mechanisms by which vertical variations in gas concentrations influence longwave radiation absorption and emission.

Traditionally, radiative forcing estimates are based on column-averaged concentrations under the assumption that greenhouse gases are vertically well mixed. While this approximation is generally reasonable at the global scale, its applicability becomes questionable in regions characterized by strong stratification and unique thermodynamic structures. In such cases, neglecting the vertical inhomogeneity of greenhouse gases may introduce systematic biases in the estimation of radiative forcing responses associated with vertical distribution effects, as well as in regional radiative budgets and climate impacts.

The Arctic is one of the most climate-sensitive regions on Earth and has

experienced a warming rate significantly higher than the global average, a phenomenon known as Arctic amplification. The Arctic atmosphere exhibits distinct characteristics, including low aerosol loading, stable stratification, strong temperature inversion in the stratosphere, and relatively low water vapor content. These features make longwave radiative processes more sensitive to greenhouse gas perturbations. Under such conditions, differences in greenhouse gas concentrations between the troposphere and stratosphere can significantly alter layer-by-layer radiative forcing responses and the net radiative flux at the top of the atmosphere[1].

In the context of intensifying climate change and the advancement of carbon neutrality goals, accurately quantifying the radiative forcing responses induced by greenhouse gas vertical distributions is essential for understanding climate system responses and improving future climate projections. Moreover, under low-emission scenarios such as Shared Socioeconomic Pathway 1-2.6 (SSP1-2.6), greenhouse gas concentrations may stabilize or decline, while atmospheric temperature and water vapor still change significantly. These changes may further modulate the sensitivity of radiative forcing responses to vertical gas distributions, leading to radiative responses that differ from those under present-day conditions.

Therefore, systematically investigating the radiative forcing responses induced by the vertical distribution of greenhouse gases, especially in the Arctic region, is of great scientific significance. Such studies not only help overcome the limitations of the traditional column-averaged assumption, but also improve the physical understanding of altitude-dependent radiative processes, refine parameterization schemes in climate models, and enhance the reliability of climate projections under future scenarios. Ultimately, this contributes to a more accurate assessment of regional climate change and provides scientific support for climate mitigation and policy-making.

1.2 Current research status

Radiative forcing is a primary driver of global warming and has significant

impacts on human society; accordingly, extensive research has been conducted in this field. IPCC AR6 clearly indicates that radiative forcing has increased continuously since 1750 and has accelerated in recent decades[2]. Research based on satellite observations have shown that global all-sky radiative forcing increased continuously from 2003 to 2018, mainly driven by rising concentrations of well-mixed greenhouse gases and the combined effects of reflective aerosols[3]. This indicates that human activities have substantially altered the Earth's radiative energy balance, highlighting the importance of radiative forcing research.

Among the contributors to radiative forcing, aerosols in the mid and low latitude regions, due to their relatively high concentrations, exert a significant cooling effect on the climate system. As a result, many previous studies have focused on aerosol radiative forcing. However, recent studies suggest that the cooling effect of aerosols (negative effective radiative forcing, ERF) is weakening or even reversing[4], implying a diminishing role of aerosols in offsetting global warming. Under this context, the positive radiative forcing induced by greenhouse gases becomes increasingly prominent, further emphasizing the necessity of studying their radiative effects.

In terms of quantitative estimation, the IPCC has proposed a series of simplified expressions for radiative forcing based on long-term experience, allowing direct calculation from column-mean concentrations of greenhouse gases and aerosols[5]. However, studies based on high-resolution line-by-line radiative transfer models indicate that such simplified parameterizations may underestimate the radiative forcing of certain gases; for example, the forcing of CH_4 can be underestimated by approximately 25% relative to line-by-line calculations[6]. This highlights the significant uncertainties associated with concentration-based simplified approaches.

To improve the accuracy of radiative forcing calculations, an increasing number of studies have adopted radiative transfer models. The Rapid Radiative Transfer Model (RRTM) and the Rapid Radiative Transfer Model for GCMs (RRTMG) employ efficient algorithms to achieve near line-by-line accuracy while maintaining computational efficiency, and are therefore widely used in climate models[7][8]. Previous studies have shown that radiative forcing depends not only on gas

concentrations but is also strongly influenced by water vapor content and temperature structure; in cold and dry regions, negative top-of-atmosphere (TOA) radiative forcing may even occur[9][10]. This demonstrates that the background atmospheric state is a key factor controlling radiative responses.

However, most of the aforementioned studies are based on the assumption of column-mean concentrations, implying that greenhouse gases are vertically well mixed. Observational evidence suggests that this assumption does not hold in the real atmosphere. Aircraft measurements and ground-based retrievals both indicate significant vertical inhomogeneities in CO_2 and CH_4 over the Arctic region[11][12].

Further studies have demonstrated that the vertical structure of greenhouse gases can significantly affect radiative forcing estimates. For long-lived, nearly well-mixed gases (such as CO_2 and CFC-12), the use of a single global mean profile can still introduce errors of several percent, while the use of regionally differentiated profiles can substantially reduce these errors. The sensitivity to vertical distribution varies notably with gas lifetime. In general, neglecting vertical structure leads to errors of about 10% in global mean radiative forcing for long-lived gases, whereas for short-lived gases with pronounced vertical gradients, the errors can reach up to 30%. It has been shown that these errors arise primarily from vertical, rather than horizontal, inhomogeneities, with the rate of concentration decrease above the tropopause being a key controlling factor. In addition, although some gases (e.g., CH_4) exhibit near-surface inhomogeneities, their impact on global mean radiative forcing is relatively small (typically less than 2%), whereas larger regional biases may still occur at high latitudes. Overall, the vertical distribution of greenhouse gases plays a crucial role in radiative forcing estimation, particularly at regional scales[13].

To quantitatively assess contributions from different atmospheric layers, sensitivity kernel methods have been developed, in which uniform perturbations are applied at different altitudes to diagnose the vertical structure of TOA radiative forcing responses[14]. Moreover, studies have shown that under identical greenhouse gas concentration conditions, variations in temperature and water vapor profiles can significantly alter radiative forcing[15], further highlighting the dependence of

radiative processes on atmospheric structure.

From a regional perspective, the Arctic exhibits radiative characteristics that are markedly different from those of mid- and low-latitude regions. Due to relatively low aerosol concentrations, the radiative cooling effect of aerosols is weaker in the Arctic [16][17], making greenhouse gas radiative effects more prominent. At the same time, greenhouse gas vertical distributions in the Arctic display strong regional and seasonal variability[18], accompanied by pronounced temperature inversions and low water vapor content, which enhance the sensitivity of radiative processes to vertical structure. Previous studies investigating longwave radiative differences under doubled greenhouse gas concentrations between the Arctic and other regions have shown that, under polar conditions, radiative forcing depends not only on concentration but is also strongly modulated by the vertical structures of temperature and water vapor[19].

In the context of future climate change, the evolution of radiative forcing has also received extensive attention. The IPCC AR6 and related studies suggest that under low-emission pathways, radiative forcing will stabilize and gradually decline [2][20][21][22]. However, most of these studies are based on changes in column-mean concentrations, with limited consideration of the role of vertical structure and its radiative effects.

In summary, although substantial progress has been made in understanding radiative forcing mechanisms and their climatic impacts, most existing studies still rely on the assumption of column-mean concentrations and neglect the influence of vertical distribution. This limitation is particularly critical in the Arctic, where low aerosol loading, stable stratification, strong temperature inversions, and low water vapor content contribute to more complex radiative processes. Nevertheless, quantitative studies on the impact of greenhouse gas vertical structure on radiative forcing in the Arctic remain limited, highlighting the need for systematic investigation.

1.3 Research content and technical route

1.3.1 Research content

This study focuses on the instantaneous clear-sky radiative forcing responses of greenhouse gases CO_2 and CH_4 under different vertical structures in the Arctic. By comparing observed profiles with uniform column-mean distributions, a set of radiative transfer experiments is designed to quantitatively evaluate the radiative forcing responses induced by the vertical inhomogeneity of greenhouse gases. On this basis, combined with background fields at different spatial scales and a future carbon neutrality scenario, the spatial representativeness of the radiative responses and their evolution mechanisms under climate change are further analyzed. According to the research content, this thesis is organized into five chapters:

Chapter 1 is the Introduction, which presents the radiative effects of greenhouse gases and the climatic characteristics of the Arctic, describes the research background and significance, and reviews related studies as well as the main content of this work.

Chapter 2 is Data and Methodology, which introduces the AirCore observational data, WACCM-X background fields, and CESM2 SSP1-2.6 scenario data, and describes the profile processing methods, the RRTMG radiative transfer calculations, and the experimental design for radiative forcing responses.

Chapter 3 presents the analysis of radiative responses to greenhouse gas vertical structures. It examines the vertical characteristics of CO_2, CH_4, as well as background temperature and water vapor profiles, calculates longwave radiative fluxes and heating rate structures, quantitatively evaluates layer-resolved and TOA radiative forcing responses, and conducts layer sensitivity analysis.

Chapter 4 focuses on spatial representativeness and carbon neutrality scenario analysis. It evaluates the effects of different background fields and spatial scales on radiative forcing responses, analyzes the regional applicability of single-site results, and compares the changes in radiative responses under the SSP1-2.6 scenario and their underlying causes.

Chapter 5 provides the conclusions and outlook, summarizing the main findings,

identifying key mechanisms, highlighting the innovations, and proposing directions for future research.

1.3.2 Technical route

The specific technical framework of this study is shown in figure 1:

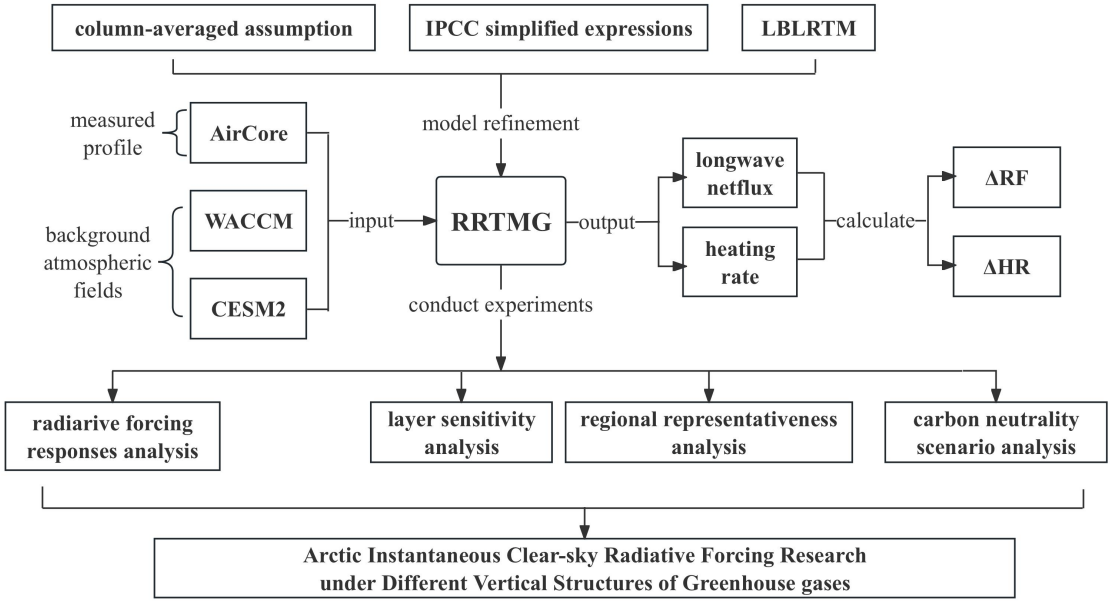

Figure.1 Technical framework for Arctic instantaneous clear-sky radiative forcing research under different greenhouse gas vertical structures

2 Data and methodology

2.1 Research data

2.1.1 AirCore observations

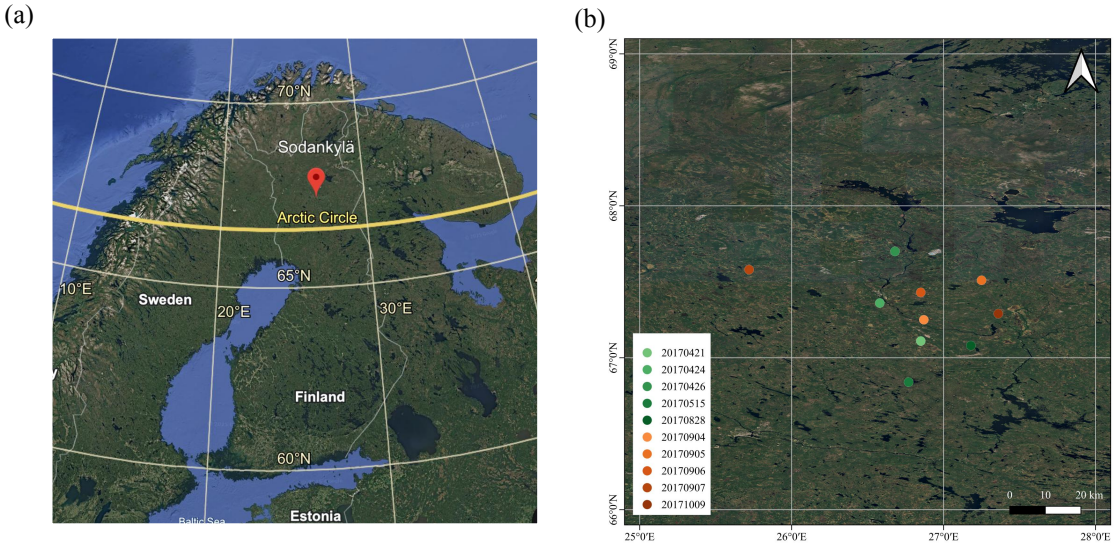

Figure.2 Geographic context and spatial distribution of AirCore profiles over Sodankylä: (a) location of the Sodankylä observation site in the Arctic, and (b) spatial distribution of landing sites derived from ten AirCore profiles (April – October 2017).

This study selects the Sodankylä region in Finland as the research site. Figure 2 shows the spatial distribution of landing sites corresponding to the ten AirCore observations. Sodankylä is located within the Arctic Circle in Finnish Lapland, at the northern edge of the Eurasian continent. Being far from the ocean and sea ice areas, it is not directly influenced by sea ice albedo effects and exhibits typical inland polar climate characteristics. The region is characterized by relatively flat terrain and homogeneous surface conditions, with stable meteorological environments, and serves as one of the key long-term observation sites for atmospheric composition and radiation in high-latitude Europe.

Sodankylä hosts a high-precision AirCore observation system that provides high-resolution vertical profiles of CO_2 and CH_4. These measurements offer a reliable data foundation for investigating the vertical distribution characteristics of greenhouse gases and their impacts on radiative forcing. Therefore, selecting this region as the study area facilitates a more accurate assessment of the contribution and modulation mechanisms of greenhouse gas vertical structure to Arctic radiative forcing under

conditions free from direct sea ice interference.

Due to incomplete sampling during the initial and final stages of the AirCore profile, some data are missing in the near-surface layer. In addition, partial data gaps also occur in the upper atmosphere due to low pressure conditions and increased measurement uncertainty.

Table.1 Geographic coordinates of landing sites corresponding to the ten AirCore profiles over Sodankylä (April–October 2017)

Date	0421	0424	0426	0515	0828	0904	0905	0906	0907	1009
Longitude	26.85	26.58	26.68	26.77	27.18	26.87	27.25	26.85	25.72	27.36
Latitude	67.11	67.36	67.7	66.84	67.08	67.25	67.51	67.43	67.58	67.29

The observational data used in this study were obtained from the Sodankylä station in Finland and were jointly provided by the University of Groningen (RUG) and the Finnish Meteorological Institute (FMI) as part of the European Space Agency (ESA) FRM4GHG project. The observations were conducted using the RUG AirCore1 system, with a total of ten high-altitude balloon launches performed between April and October 2017. The specific observation dates are listed in Table 1. The dataset provides high-resolution vertical profiles including pressure(hPa), altitude (m), CO_2 (ppm), CH_4 (ppb), CO (ppb), temperature (K), and relative humidity (%).

Since the AirCore balloon drifts horizontally with atmospheric flow during flight, the final landing site can more accurately represent the atmospheric location corresponding to each profile. Therefore, the landing site locations are used in this study to characterize the spatial distribution of the profiles. The distribution of these landing sites is shown in Figure 1, and the corresponding latitude and longitude for each profile are listed in Table 1. The dataset covers a representative period from spring to autumn, providing a reliable observational basis for analyzing the vertical structure of greenhouse gases and their radiative forcing effects in the Arctic region.

2.1.2 WACCM-X background atmosphere fields

The background atmospheric fields used for the spatial representativeness analysis are obtained from the SD WACCM-X v2.1 Atmosphere Daily Average

product. This dataset is based on simulations from the Whole Atmosphere Community Climate Model with thermosphere and ionosphere extension (WACCM-X) operating in Specified Dynamics (SD) mode[23][24]. By constraining atmospheric dynamics with reanalysis data, the model is able to realistically reproduce the dynamical and thermodynamical structures of the atmosphere from the troposphere to the middle and upper atmosphere. Consequently, WACCM-X has been widely applied in studies of atmospheric chemistry, climate change, and radiative processes.

In this study, the WACCM-X data are primarily used to provide background atmospheric fields required for radiative transfer calculations over the Arctic region, including temperature, pressure, and O_2 concentration. These data are also used to evaluate the spatial representativeness of observations from the Sodankylä site at the regional scale.

2.1.3 CESM2 SSP1-2.6 scenario simulation data

Future background atmospheric fields are obtained from simulations of the Community Earth System Model Version 2 (CESM2) provided by the Coupled Model Intercomparison Project Phase 6 (CMIP6). In this study, model outputs under the SSP1-2.6 scenario for the period 2080–2100 are selected.

CESM2 is a comprehensive Earth system model developed by the National Center for Atmospheric Research. It simulates interactions among multiple components of the Earth system, including the atmosphere, ocean, land surface, and sea ice, and has been widely used in studies of global climate change and future climate projections. The SSP1-2.6 scenario represents a typical low-emission pathway consistent with strong mitigation and carbon neutrality, and can therefore be used to assess changes in the radiative forcing response induced by the vertical structure of greenhouse gases under strong emission reduction conditions. The period 2080–2100 is selected for analysis because greenhouse gas concentrations in this stage tend to stabilize, representing a relatively steady future climate state.

The variables used in this study include air temperature (ta), surface pressure (ps),

and specific humidity (hus), which are obtained from the monthly mean atmospheric outputs (Amon) of CESM2. The O_3 concentration data are taken from simulations of CESM2-WACCM within the same CMIP6 model framework. Although there are structural differences between the two models, CESM2-WACCM is an atmospheric chemistry extension of CESM2 and shares the same dynamical framework and major physical parameterization schemes. Therefore, under the same scenario forcing, the two models exhibit good physical consistency and can be used together to construct a unified future background atmospheric field.

2.2 Research methodology

2.2.1 RRTMG radiative transfer model

RRTMG is a fast radiative transfer model developed for general circulation models (GCMs). Its radiative algorithm is based on the correlated-k distribution method, which is used to efficiently calculate atmospheric longwave (LW) and shortwave (SW) radiative fluxes and heating rates. RRTMG was developed as an accelerated and improved version of the earlier RRTM, designed to meet the requirements of long-term simulations in numerical weather prediction and climate models. In the longwave scheme, RRTMG contains 16 spectral bands, while the shortwave scheme includes 14 spectral bands, both of which apply the correlated-k distribution integration method to solve radiative transfer[7]. The model also accounts for the radiative effects of absorbing gases (including H_2O, CO_2, O_3, CH_4, and O_2) as well as cloud variables, and maintains good consistency with the widely validated line-by-line radiative transfer model (LBLRTM).

Compared with RRTM, RRTMG significantly improves computational efficiency by reducing the number of g-points (140 in the longwave scheme compared with 256 in RRTM, and 112 in the shortwave scheme compared with 224 in RRTM), while still maintaining consistency with high-resolution models. The g-points denote the discrete integration points in the correlated-k distribution method, representing different intervals of absorption coefficient probability and their contributions to

radiative transfer. A smaller number of g-points generally leads to higher computational efficiency. The scheme has been widely integrated into the radiation modules of general circulation models (GCMs) and weather prediction models such as GFS and WRF, serving as a standard spectral radiation calculation scheme[8].

After the constructed atmospheric profiles are input into the RRTMG, the model produces vertical radiative calculation results for 50 atmospheric layers over the longwave wavenumber range of 10.0–3250.0 cm^{-1}. The output variables include pressure at each layer (mbar), upward radiative flux (W m^{-2}), downward radiative flux (W m^{-2}), net radiative flux (W m^{-2}), and heating rate (K day^{-1}). The net radiative flux is defined as the upward radiative fluxes minus downward radiative fluxes. The heating rate is calculated from the vertical gradient of net radiative flux for each atmospheric layer, that is:

$$HR = -\frac{1}{\rho c_p}\frac{dF}{dz} \tag{2-1}$$

It reflects the rate of temperature change caused by the radiation process at each height layer.

2.2.2 Preparation of input data for RRTMG using AirCore profiles

The ten AirCore observations conducted at the Sodankylä station from April to October 2017 were used to construct standard atmospheric profile input files for RRTMG radiative transfer model calculations. For missing values flagged as 99999, a boundary value substitution method was applied, in which each missing value was replaced by the nearest valid observation.

Among the trace gases, N_2O, O_2, and O_3 concentrations were not available in the AirCore observations. In this study, the volume mixing ratio of N_2O was fixed at 0.33 ppm, and the volume mixing ratio of O_2 was fixed at 209500 ppm. The O_3 concentration was constructed using an idealized vertical distribution: in the troposphere ($p > 300$ hPa) it was set to 0.04 ppm, while in the stratosphere (10–300 hPa) it was assumed to increase linearly with decreasing pressure, reaching a maximum of 6 ppm. This configuration is based on previously reported vertical

distributions of ozone[25] and is intended to construct a reasonable yet simplified ozone profile, thereby minimizing the influence of non-target gases on the radiative forcing calculations.

For water vapor, the AirCore dataset only provides relative humidity (RH); therefore, the volume mixing ratio of water vapor needs to be derived. First, the saturation vapor pressure is calculated using the Tetens empirical formula:

$$e_s = 6.112 \times \exp\left(\frac{17.67 T_C}{T_C + 243.5}\right) \tag{2-2}$$

where T_C is the temperature in degrees Celsius.

The actual vapor pressure is then calculated as:

$$e = RH \times e_s \tag{2-3}$$

Finally, the volume mixing ratio is obtained according to the ideal gas relationship:

$$\mathrm{H_2O_{ppm}} = \frac{e}{P} \times 10^6 \tag{2-4}$$

where P is the ambient pressure (hPa).

The original AirCore data have high and uneven vertical resolution, which is not suitable for direct input into the RRTMG. To improve computational efficiency and ensure the stability of radiative integration, the profiles were resampled to 50 pressure levels uniformly spaced in logarithmic pressure space, from which 49 atmospheric layers were defined by adjacent levels.

$$p_i = \exp\left[\ln(p_{\mathrm{bottom}}) + \frac{i}{N-1}\left(\ln(p_{\mathrm{top}}) - \ln(p_{\mathrm{bottom}})\right)\right] \tag{2-5}$$

where N = 50.

Subsequently, temperature, water vapor, and all trace gas concentrations were interpolated onto the new pressure levels using linear interpolation.

Table.2 Summary of variables and units in AirCore raw data and corresponding RRTMG input data

AirCore raw data	name	/	P	CO_2	CH_4	CO	/	/	/	T	RH	Altitude
	unit	/	hPa	ppm	ppb	ppb	/	/	/	K	%	m
Input data	name	Layer Index	P	CO_2	CH_4	CO	O_3	N_2O	O_2	T	H_2O	Attitude
	unit	/	hPa	ppm	ppm	ppm	ppm	ppm	ppm	K	ppm	km

Table 2 presents the correspondence between the variables in the AirCore raw data and those in the RRTMG input data. The final input files were constructed based on the variables listed in Table 2 and were used for subsequent radiative forcing calculations with RRTMG.

2.2.3 Radiative forcing experiments for observed and uniform GHG profiles

To investigate the modulation effect of vertical distributions of greenhouse gases on radiative forcing in the Sodankylä region in 2017, this study considers two scenarios for CO_2 and CH_4: an 'actual vertical profile' and an 'equivalent column-mean uniform distribution.' Comparative experiments between the observed profile distribution and the uniform distribution are conducted using the RRTMG model. The experimental design is described as follows.

Experiment 1: The input file described in Section 2.2.1 is used as the input to RRTMG to calculate the net radiative flux and heating rate under the observed greenhouse gas vertical profile, denoted as $F_{profile}$ and $HR_{profile}$, respectively.

Experiment 2: The greenhouse gas concentrations in the input file are vertically homogenized, while other atmospheric variables remain unchanged. The net radiative flux and heating rate under the uniform distribution condition is calculated, denoted as $F_{uniform}$ and $HR_{uniform}$, respectively.

The difference in net radiative flux between the two experiments is defined as the radiative forcing responses induced by the vertical structure (ΔRF), expressed as:

$$\Delta RF(p) = F_{\mathrm{uniform}}(p) - F_{\mathrm{profile}}(p) \quad (2\text{-}6)$$

Where ΔRF(p) denotes the difference in net radiative flux between the two scenarios at pressure level p. Because the net radiative flux at a given altitude already incorporates the combined effects of radiative absorption, emission, and transfer from all underlying atmospheric layers, the vertical profile of ΔRF reflects the cumulative radiative response up to that altitude. As altitude increases, the radiative effects from different layers progressively accumulate and ΔRF gradually approaches a stable value. Therefore, the ΔRF at the top of the atmosphere, denoted as ΔRF_{TOA}, can be regarded as the total radiative forcing response of the entire atmospheric column

induced by the vertical inhomogeneity of greenhouse gas distributions.

According to the definition of ΔRF in Eq. (2–5), all radiative forcing responses are expressed as the net longwave radiative flux under the uniform profile minus that the observed profile. When ΔRF is negative ($F_{uniform} < F_{profile}$), it indicates that the uniform distribution will underestimate the outgoing longwave radiation. Conversely, when ΔRF is positive ($F_{uniform} > F_{profile}$), it indicates that the uniform distribution will overestimate the outgoing longwave radiation.

Similarly, the difference in heating rate is defined as the heating rate change induced by the vertical structure (ΔHR), expressed as:

$$\Delta HR(p) = HR_{\text{uniform}}(p) - HR_{\text{profile}}(p) \quad (2\text{-}7)$$

Where ΔHR(p) represents the local heating rate change at pressure level p caused by the non-uniform vertical distribution of greenhouse gases. Since the atmospheric heating rate is fundamentally determined by the vertical gradient of the net radiative flux, Δ HR effectively reflects the vertical variation of ΔRF, i.e., the local heating or cooling response at different altitude levels resulting from differences in radiative energy balance.

According to the definition of ΔHR in Eq. (2–7), all heating rate changes are expressed as the heating rate under the uniform greenhouse gas profile minus that under the observed profile. When ΔHR is positive ($HR_{uniform} > HR_{profile}$), it indicates that the uniform distribution assumption leads to an enhanced local heating rate relative to the observed vertical profile. Conversely, when ΔHR is negative ($HR_{uniform} < HR_{profile}$), it indicates that the uniform distribution assumption leads to a reduced local heating rate.

Based on these definitions, the radiative forcing response profiles and heating rate response profiles of CO_2 and CH_4 under the observed vertical distribution and the equivalent column-mean uniform distribution scenarios can be obtained.

2.2.4 Layer sensitivity kernel method

To quantitatively characterize the altitude dependence of radiative forcing responses induced by changes in the vertical profile distribution of greenhouse gases,

this study further introduces the Layer Sensitivity Kernel method[26][27]. This method evaluates the TOA net longwave radiative response caused by a unit concentration perturbation of greenhouse gases at different altitude levels, thereby quantifying the contribution of each layer to the total radiative forcing and identifying the key layers most sensitive to radiative forcing.

Specifically, under the condition that the vertical distributions of all other atmospheric state variables (temperature, pressure, water vapor and concentrations of other gases) unchanged, a small positive perturbation ΔC is applied to the CO_2 or CH_4 concentration in the i-th atmospheric layer. The perturbation magnitude is set to 1 ppm for CO_2 and 10 ppb for CH_4. The TOA net longwave radiative flux before and after the perturbation is then calculated using RRTMG-LW. The resulting change in TOA radiative flux for that layer can be expressed as:

$$\Delta F_i = F^{\mathrm{pert}}_{\mathrm{TOA},\,i} - F^{\mathrm{bg}}_{\mathrm{TOA},\,i} \tag{2-8}$$

where $F^{bg}TOA,i$ represents the TOA net longwave radiative flux under the background atmospheric profile, and $F^{pert}TOA,i$ represents the TOA net longwave radiative flux after applying the concentration perturbation only in the i-th layer.

The layer radiative sensitivity kernel for the i-th layer is then defined as:

$$K_i = \frac{\Delta F_i}{\Delta C} \tag{2-9}$$

Physically, K_i represents the radiative forcing response at the TOA caused by a unit concentration change of greenhouse gas in that specific atmospheric layer, with units of W m^{-2} ppm^{-1}. This quantity directly reflects the contribution of different altitude layers to the TOA radiative forcing.

By calculating K_i for all vertical layers, the sensitivity distribution of radiative forcing to changes in the vertical structure of greenhouse gases can be systematically evaluated, thereby identifying the key altitude layers that play a dominant role in the radiative energy balance of the Arctic region.

2.2.5 Spatial representativeness analysis

To evaluate whether the single-station results exhibit consistency at the Arctic

regional scale, this study assesses the differences in radiative forcing responses induced by the vertical distributions of CO_2 and CH_4 across multiple spatial scales. The background atmospheric field data used in this study are obtained from simulations conducted with WACCM. This study selected September 7, 2017, as the experimental date, when both WACCM and AirCore had data coverage, to ensure the consistency of the background field and the observed profile.

The comparison experiments between the observed greenhouse gas vertical profiles and the equivalent column-mean uniform distributions are repeated at three different spatial scales. These include the single WACCM grid cell containing the Sodankylä Observatory station (26.63° E, 67.37° N), a $\pm 2.5°$ latitude–longitude region centered on the station, and the entire Arctic region. Across these spatial scales, the vertical distributions of greenhouse gases and other trace gases were kept unchanged, while only temperature and pressure fields were allowed to vary.

If the radiative forcing results across different spatial scales show good agreement in both vertical structure and magnitude, this indicates that the radiative forcing response derived from single station AirCore observations has a certain degree of spatial representativeness, and that the conclusions regarding the influence of greenhouse gas vertical distributions on radiative forcing can be reasonably extended to a broader Arctic regional scale.

2.2.6 Experimental Design under the SSP1-2.6 Scenario

Under the background of global emission reductions and the advancement of carbon neutrality pathways, both future greenhouse gas concentrations and the background atmospheric state are expected to undergo significant changes. In this study, comparative experiments between the observed vertical profiles and uniform distributions of greenhouse gases are designed under a carbon neutrality scenario to investigate whether radiative forcing responses induced by the greenhouse gases vertical structure remains significant under low emission conditions.

To achieve this objective, the SSP1-2.6 scenario adopted in IPCC Sixth Assessment Report (AR6)[2] is introduced, and output data from the CESM2 and

CESM2-WACCM models are used to construct the future background atmospheric field.

The experimental design is as follows. First, the radiative forcing responses induced by the vertical structures of CO_2 and CH_4 in 2017 are divided into two representative seasonal profiles: spring (21 April, 24 April, 26 April, and 15 May) and autumn (28 August, 4 September, 5 September, 6 September, 7 September, and 9 October). Based on the AirCore observational profiles obtained at the Sodankylä Observatory station in 2017, the column-mean concentrations of CO_2 and CH_4 are calculated separately for spring and autumn. The RRTMG is then used to perform four sets of comparative experiments between the observed vertical profiles and the equivalent column-mean uniform distributions of greenhouse gases, yielding four vertical radiative forcing responses profiles(i.e., spring CO_2, spring CH_4, autumn CO_2, and autumn CH_4).

Next, the radiative forcing responses induced by the vertical structures of CO_2 and CH_4 are analyzed under the SSP1-2.6 scenario, using the multi-year mean conditions for spring and autumn during 2080–2100. The study location is chosen as the grid point closest to Sodankylä. In the input files, CO is prescribed using an idealized vertical profile that decreases linearly from 0.1 ppm near the surface to 0.03 ppm in the upper atmosphere. The volume mixing ratio of N_2O is fixed at 0.35 ppm, and that of O_2 is fixed at 209500 ppm. These gases are primarily included to ensure the completeness of the radiative transfer calculations, and their variations have minimal influence on the radiative forcing response differences associated with the vertical structures of CO_2 and CH_4 examined in this study. Temperature, specific humidity, and pressure are obtained from the CESM2 model outputs, while O_3 is taken from the CESM2-WACCM simulations. The altitude profile is derived from pressure using the hydrostatic equilibrium equation.

For CO_2 and CH_4 concentrations, the global mean concentrations corresponding to the SSP1-2.6 scenario in IPCC AR6 (CO_2 = 456.67 ppm, CH_4 = 1121.67 ppb) are used. For CH_4, the 2017 AirCore profiles are uniformly scaled while preserving their original vertical structure, such that the column-mean concentration matches the

target value. For CO_2, under the carbon neutrality scenario, the vertical gradient in the stratosphere is expected to be significantly weakened or even disappear, whereas in the troposphere, CO_2 is likely to maintain a relatively stable vertical distribution due to the continuous uptake and release of carbon by the biosphere. Accordingly, a layer-wise construction method is applied to CO_2 in this study: the original vertical structure is preserved and proportionally scaled within the troposphere, while in the stratosphere, CO_2 is set to a constant value equal to that at the tropopause. After that, the CO_2 profile is normalized using pressure-weighted averaging to ensure that the column-mean concentration is consistent with the IPCC projected value.

After constructing the complete future atmospheric input profiles, the RRTMG model is again applied to perform four sets of comparative experiments between the observed and uniform distributions of greenhouse gases, producing four vertical radiative forcing responses profiles associated with CO_2 and CH_4 under spring and autumn conditions in the SSP1-2.6 scenario.

By comparing the eight radiative forcing profiles obtained from the two periods (2017 and 2080–2100), the study systematically analyzes how changes in total greenhouse gas concentrations and background climate conditions modulate the radiative responses associated with vertical structure.

3 Radiative responses to CO_2 and CH_4 vertical structure

3.1 Vertical structure of atmospheric profiles

To understand how greenhouse gas vertical structures influence radiative processes, it is first necessary to examine the observed atmospheric profiles over the study region. This section presents the vertical distributions of CO_2, CH_4, temperature, and water vapor derived from AirCore observations over Sodankylä, which provide the observational atmospheric background for the subsequent radiative transfer analysis.

3.1.1 CO_2 and CH_4 profiles

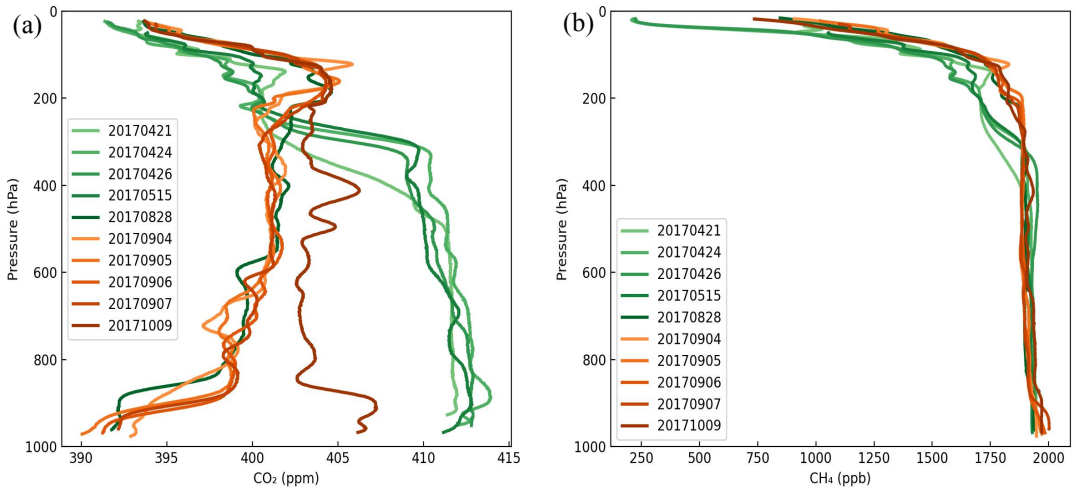

Figure.3 Vertical profiles over Sodankylä derived from AirCore observations (a) CO_2 concentration (b) CH_4 concentration

Figure 3(a) and (b) present the vertical profiles of CO_2 and CH_4 over Sodankylä. It can be seen that both gases exhibit pronounced vertical inhomogeneity. In the CO_2 profiles, during spring (April–May), CO_2 concentrations in the troposphere (below approximately 300 hPa) generally remain above 410 ppm, indicating strong contributions from surface biological respiration and soil emissions. From the troposphere top to the stratosphere (around 200–300 hPa), CO_2 concentrations decrease rapidly to approximately 400 ppm, mainly due to dilution by stratospheric air and limited exchange across the tropopause.

In contrast, during summer (August–October), the profile characteristics are reversed. Surface CO_2 concentrations are lower (approximately 390–395 ppm) and gradually increase with altitude, reaching a maximum about 405ppm near the tropopause (around 200 hPa). This pattern reflects enhanced photosynthetic uptake in the lower troposphere during summer, while higher altitudes are more strongly influenced by stratospheric air mixing and cross-latitudinal transport.

For CH_4, concentrations are relatively high throughout the troposphere (approximately 1900–2000 ppb). Near the tropopause and in the lower stratosphere, CH_4 concentrations gradually decrease with increasing altitude, reflecting its primary sources at the surface, including peatlands and freshwater ecosystems. In spring, the profile shows a more pronounced decrease in the upper troposphere to lower stratosphere (approximately 400–200 hPa). This feature is more likely associated with descending air under the influence of the polar vortex, which transports methane-poor stratospheric air downward to lower altitudes, rather than being solely caused by weakened vertical mixing in the troposphere. In contrast, during summer, enhanced convection and turbulence lead to a weaker vertical gradient of CH_4, with relatively higher concentrations at upper levels, indicating more efficient vertical mixing.

Table.3 Average CO_2 and CH_4 concentrations derived from individual AirCore profiles over Sodankylä (April – October 2017).

Date	0421	0424	0426	0515	0828	0904	0905	0906	0907	1009
CO_2 Mean value (ppm)	406.89	407.94	407.35	408.18	399.39	399.24	399.17	399.90	399.80	403.30
CH_4 Mean value (ppb)	1801.6	1799.9	1805.3	1836.2	1846.3	1853.8	1852.7	1867.3	1848.8	1856.3

The mean concentrations of each CO_2 and CH_4 vertical profile are listed in Table 3. It can be seen that the average CO_2 concentrations in April–May and October are all above 400 ppm, whereas values in August–September are relatively lower. Unlike CO_2, the mean CH_4 concentration shows a pronounced increase from April to October, rising gradually from about 1800 ppb in spring to approximately 1850–1870 ppb in autumn. The data in the table are further used to construct the uniform distribution

scenarios and are then input into the RRTMG model to calculate the net radiative flux and heating rate of CO_2 and CH_4 under uniform distribution conditions.

3.1.2 Temperature and water vapor profiles

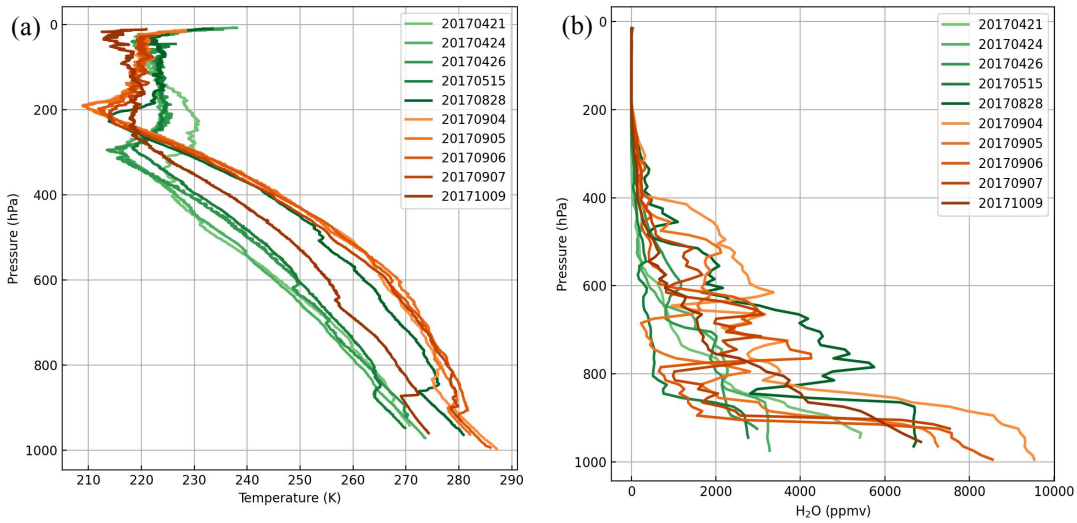

Figure.4 Vertical profiles over Sodankylä derived from AirCore observations (a) temperature (b) water vapor concentration

Figure 4(a) presents the vertical profiles of temperature over Sodankylä. It can be seen that the overall thermal structure follows the typical atmospheric stratification pattern: temperature decreases with height in the troposphere and increases with height in the stratosphere, exhibiting a clear tropospheric lapse rate and a pronounced stratospheric temperature inversion.

Significant seasonal differences in the atmospheric thermodynamic structure are evident. In spring (April–May), the tropopause is located at approximately 300 hPa, slightly lower than in autumn (September–October), when it rises to around 200 hPa. In addition, the rate of temperature decrease with altitude in the spring troposphere is relatively weaker, indicating more stable stratification and weaker vertical mixing. In contrast, the tropospheric lapse rate in autumn is larger, reflecting a stronger vertical temperature gradient and relatively enhanced dynamical activity. The stratospheric temperature inversion in autumn is more pronounced than in spring, suggesting relatively stronger radiative heating in the upper atmosphere and more stable stratification above the tropopause.

Figure 4(b) presents the vertical profiles of water vapor over Sodankylä. The

overall trend of water vapor concentration in all seasons shows a decrease with increasing altitude, exhibiting a typical near-surface enrichment characteristic. Compared with spring, autumn shows slightly higher water vapor content in parts of the lower atmosphere below 400 hPa, reflecting the combined effects of surface evaporation and the retention of moisture in the near-surface layer during autumn.

Under stable stratification, water vapor tends to accumulate in the lower atmosphere and is difficult to transport upward, thereby increasing the longwave optical thickness of the atmosphere and further affecting the radiative transfer process.

3.2 Radiative flux and heating rate structure

Based on the observed atmospheric profiles described above, radiative transfer calculations are performed to investigate the vertical structure of longwave radiative fluxes and atmospheric heating rates. These quantities provide key diagnostics for understanding how greenhouse gases modulate the vertical energy balance of the atmosphere.

3.2.1 Vertical structure of longwave net radiative flux

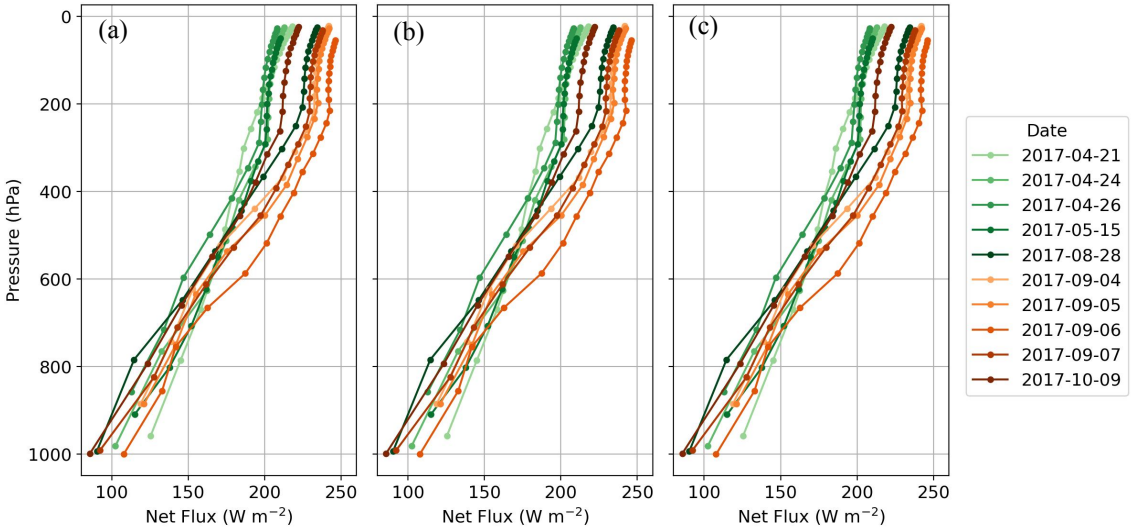

Figure.5 Vertical profiles of net radiation flux under different distribution scenarios: (a) observed vertical profiles (b) uniformly CO_2 distributed (c) uniformly distributed CH_4.

Figure 5 illustrates the vertical distribution of net longwave radiative flux under three conditions: the observed greenhouse gas vertical profile (a), a vertically uniform

distribution of CO_2 (b), and a vertically uniform distribution of CH_4 (c). The net longwave radiative flux is defined as the difference between upward and downward longwave radiation, with the positive direction defined as upward.

Under all scenarios, the net radiative flux remains positive throughout the atmospheric column, indicating that upward longwave radiation exceeds atmospheric back radiation. Overall, the net radiative flux increases with altitude. In the near-surface layer, where atmospheric density and greenhouse gas concentrations are relatively high, enhanced atmospheric back radiation results in relatively small net upward radiative fluxes (approximately 85–125 W m^{-2}). In contrast, in the upper atmosphere where the air is thinner and back radiation is weaker, the net radiative flux increases substantially, reaching values of about 200–250 W m^{-2}.

Compared with spring (April–May), the increase in net radiative flux with altitude is more pronounced in autumn (August–October). This difference is mainly related to the stronger temperature gradients and higher tropopause height in autumn, which raise the effective emission level of longwave radiation. When combined with the vertical profiles of CO_2 and CH_4, it can be observed that CO_2 concentrations in the troposphere are relatively lower in autumn, while CH_4 concentrations are enhanced in the middle and upper troposphere. These variations modify the vertical structure of longwave absorption and emission. Near the surface, the reduction in CO_2 absorption weakens atmospheric back radiation, whereas in the middle and upper troposphere, enhanced absorption and re-emission by CH_4 strengthen the upward longwave radiation relative to atmospheric back radiation. As a result, the difference between upward and downward longwave radiation becomes larger with altitude, leading to a more pronounced increase in net radiative flux in autumn.

3.2.2 Heating rate characteristics

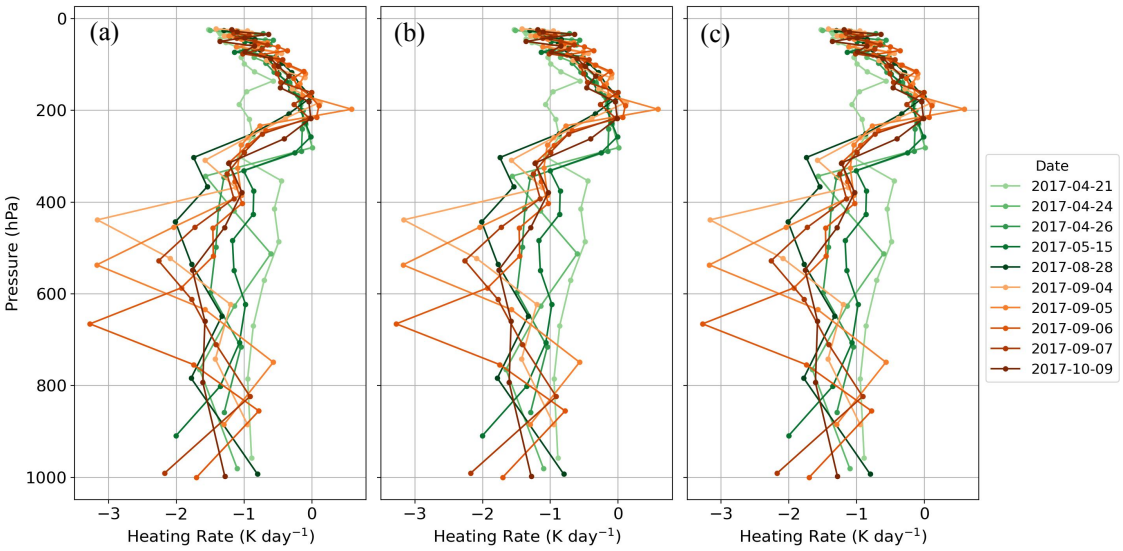

Figure.6 Vertical profiles of heating rate under different distribution scenarios: (a) observed vertical profiles (b) uniformly CO_2 distributed (c) uniformly distributed CH_4.

Figure 6 shows the vertical distribution of atmospheric heating rates under three conditions: (a) the observed vertical distribution of greenhouse gases, (b) a uniform distribution of CO_2 concentration, and (c) a uniform distribution of CH_4 concentration. Overall, the heating rate is negative throughout the entire altitude range, indicating that longwave radiative processes lead to net atmospheric radiative cooling.

In the lower atmosphere, from the surface to approximately 400 hPa, the heating rate exhibits relatively large negative values, indicating strong radiative cooling. As altitude increases, the magnitude of the negative heating rate gradually decreases, reaching the weakest cooling near about 200 hPa. Above this level, the magnitude of the negative heating rate increases again with height. This vertical structure is closely related to the distribution of the vertical divergence of net longwave radiative flux. In the lower atmosphere, the net longwave radiative flux changes rapidly with height, resulting in a large radiative flux divergence and thus strong radiative cooling. In the middle and upper atmosphere, due to reduced water vapor content and lower concentrations of absorbing gases, the absorption and emission of longwave radiation weaken, leading to a smaller vertical divergence of net radiative flux and hence weaker radiative cooling. Above approximately 200 hPa, the significant decrease in stratospheric water vapor and atmospheric optical thickness allows longwave

radiation to escape more efficiently to space, increasing the vertical divergence of net longwave radiative flux and thereby enhancing radiative cooling.

In addition, the heating rate exhibits a pronounced seasonal contrast in the lower atmosphere. Compared with spring (April to May), stronger longwave radiative cooling is observed below 400 hPa in autumn (September to October). This difference is primarily associated with the combined effects of the temperature structure and water vapor distribution. As shown in Figure 4(a), temperatures in this altitude range are generally higher in autumn than in spring. The higher temperature significantly enhances the longwave radiative emission of the atmosphere, thereby increasing the upward longwave radiative flux. Meanwhile, Figure 4(b) indicates that water vapor concentrations in the lower atmosphere are higher in autumn than in spring at certain levels. The increased water vapor enhances the longwave optical thickness of the atmosphere, making longwave radiation from lower layers more likely to be absorbed. As a result, radiative processes at each level become more strongly controlled by local thermodynamic conditions. Under such conditions, longwave emission at a given level is more strongly determined by the local temperature, which modifies the vertical distribution of the upward radiative flux.

With the combined effects of higher temperature and increased water vapor, the upward net longwave radiative flux increases more rapidly with height, leading to a larger vertical gradient of radiative flux. According to the relationship between heating rate and the vertical divergence of radiative flux, a larger flux gradient corresponds to a more negative heating rate, thereby resulting in stronger radiative cooling in the lower atmosphere during autumn.

3.3 Radiative forcing responses to GHG vertical structure

To quantitatively assess the impact of the vertical inhomogeneity of greenhouse gases on radiative processes, radiative transfer contrast experiments are conducted by comparing the observed vertical profiles with equivalent column-mean uniform distributions. This experimental design allows the radiative effects induced by the

vertical structure of greenhouse gases to be isolated.

3.3.1 Vertical distribution of ΔRF

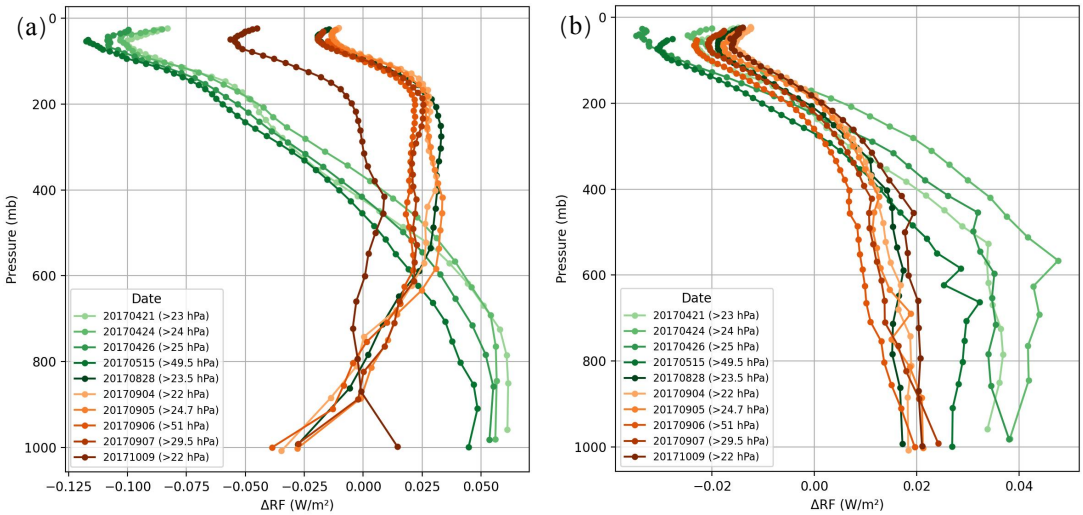

Figure.7 Vertical distribution of ΔRF associated with CO_2 (a) and CH_4 (b)

Figure 7 presents the layer-resolved cumulative radiative forcing responses of CO_2 and CH_4 under the observed vertical profiles and the column-mean uniform distribution.

In Figure 7(a), the layer-resolved ΔRF of CO_2 exhibits a pronounced seasonal dependence, with distinct differences in its vertical structure between spring and autumn, reflecting the strong modulation of radiative fluxes by seasonal variations in CO_2 vertical distribution.

In spring (April–May), the ΔRF of CO_2 shows a typical "positive in the lower layers and negative in the upper layers" structure. From the near surface to the lower–middle troposphere (approximately 1000–400 hPa), ΔRF decreases gradually from about 0.05 W m^{-2} with increasing altitude. Around the middle–upper troposphere (~400 hPa), ΔRF transitions from positive to negative, reaching a minimum near 100 hPa, with values lower than -0.1 W m^{-2}, indicating enhanced emission of net longwave radiation to space. This implies that under the actual CO_2 vertical distribution in spring, radiative energy is more effectively retained in the lower atmosphere, while the upper atmosphere favors enhanced radiative emission.

As shown in Figure 3(a), this vertical structure of ΔRF is primarily attributed to

the vertical distribution of CO_2. In spring, CO_2 concentrations near the surface are generally higher than the column mean, reflecting the combined effects of enhanced biological respiration and weak boundary layer mixing, which promote accumulation in the lower atmosphere and strengthen the absorption of upward longwave radiation, resulting in positive ΔRF. In contrast, at and above the tropopause, CO_2 concentrations are significantly lower than the column mean, reducing longwave absorption and allowing more radiation to escape to space, thereby producing negative ΔRF in the upper layers. The coexistence of lower-level enrichment and upper-level depletion leads to the pronounced vertical contrast in CO_2 radiative forcing responses in spring.

In contrast, during late summer to autumn (August–October), the vertical distribution of CO_2 radiative forcing responses becomes much more uniform, with a significantly weaker overall magnitude. During this period, ΔRF near the surface is mostly weakly negative and gradually transitions to weak positive values with increasing altitude, reaching a maximum of about 0.025 W m^{-2} in the middle–upper troposphere (approximately 600–200 hPa). Above 100 hPa, ΔRF becomes weakly negative again, indicating a much weaker modulation of radiative fluxes by CO_2 vertical structure.

This change can also be explained by the seasonal evolution of CO_2 profiles. As shown in Figure 3(a), the vertical distribution of CO_2 in autumn is more uniform. On the one hand, strong photosynthetic uptake reduces near-surface CO_2 concentrations; on the other hand, enhanced convective activity and a deeper boundary layer strengthen vertical mixing, reducing concentration gradients between lower and middle layers. Under these conditions, deviations between observed CO_2 concentrations and the column mean are reduced across all altitudes, weakening the vertical redistribution of radiative absorption and emission, and thus decreasing both the vertical gradient and seasonal differences of ΔRF.

Overall, CO_2 radiative forcing responses in the Arctic exhibit a clear seasonal control: in spring, the coexistence of lower-level enrichment and upper-level depletion leads to a pronounced structure of lower-level positive and upper-level

negative, whereas in autumn, as the vertical distribution becomes more uniform, the vertical contrast in radiative forcing is significantly reduced. This indicates that, in the Arctic, CO_2 radiative forcing depends not only on column-mean concentration but is strongly influenced by seasonally varying vertical structure.

In Figure 7(b), the layer-resolved ΔRF of CH_4 is generally positive throughout the troposphere and negative in the stratosphere, gradually transitioning from positive to negative with increasing altitude. As shown in Figure 3(b), this pattern is mainly driven by the vertical inhomogeneity of CH_4 concentration. Observations indicate that CH_4 concentrations are relatively high in the troposphere with weak vertical variation, resulting in values generally higher than the column mean, while in the stratosphere, CH_4 decreases rapidly and becomes significantly lower than in the uniform distribution.

In the troposphere, higher CH_4 concentrations enhance the absorption of upward longwave radiation and strengthen atmospheric back radiation, thereby reducing the upward net radiative flux and producing positive ΔRF. In contrast, in the stratosphere, where observed CH_4 concentrations are much lower than in the uniform case, the reduced longwave absorption allows more radiation to escape to space, leading to a rapid decrease in ΔRF with altitude.

From a seasonal perspective, CH_4 radiative forcing responses show clear differences between spring and autumn in the lower and middle troposphere. Within approximately 1000–200 hPa, ΔRF in spring (April–May) is generally larger than in autumn (August–October), while above 200 hPa, the magnitude of negative ΔRF is also slightly greater in spring. This difference is mainly associated with the lower-level accumulation of CH_4 in spring. As shown in Figure 3(b), under stable boundary layer conditions and weak vertical mixing, CH_4 from surface emissions and background transport tends to accumulate in the lower atmosphere, resulting in concentrations below 400 hPa that are significantly higher than the column mean. This enhances longwave absorption in the lower atmosphere and leads to stronger positive radiative forcing.

In contrast, ΔRF below 200 hPa is weaker in autumn, and the difference between

spring and autumn becomes much smaller within 0–200 hPa. This is likely associated with stronger tropospheric mixing and vertical transport in autumn, which reduce the vertical gradient of CH_4 and lead to a more vertically homogeneous distribution. Seasonal variations in CH_4 chemical loss may also contribute to changes in the vertical structure, thereby weakening the modulation of ΔRF by non-uniform CH_4 distributions.

Overall, CH_4 radiative forcing responses are stronger in the lower atmosphere in spring, while in autumn they exhibit a smoother vertical distribution, indicating that the seasonal variation of CH_4 ΔRF is largely controlled by the balance between lower-level accumulation and vertical mixing intensity.

3.3.2 TOA ΔRF

Table.4 TOA longwave radiative forcing responses induced by vertical distribution of CO_2 and CH_4 over Sodankylä (April–October 2017).

Date	0421	0424	0426	0515	0828	0904	0905	0906	0907	1009
CO_2 ΔRF_{TOA} ($W\ m^{-2}$)	-0.0831	-0.0853	-0.0997	-0.1168	-0.0144	-0.0105	-0.0118	-0.0151	-0.0171	-0.0451
CH_4 ΔRF_{TOA} ($W\ m^{-2}$)	-0.0149	-0.0200	-0.0337	-0.0277	-0.0145	-0.0125	-0.0140	-0.0229	-0.0176	-0.0140

Table 4 presents the ΔRF_{TOA} induced by the observed vertical profiles of CO_2 and CH_4 relative to the column-mean uniform distribution for different dates in 2017. Due to missing data in the upper atmosphere in some AirCore profiles, ΔRF_{TOA} in this study is defined as the ΔRF value at the top layer of the radiative forcing response profile after excluding numerically unstable high-altitude layers.

The results show that ΔRF_{TOA} for both CO_2 and CH_4 is negative for all 10 profiles in 2017. Specifically, CO_2 ΔRF_{TOA} ranges from −0.1168 to −0.0105 W m^{-2}, while CH_4 ΔRF_{TOA} ranges from −0.0337 to −0.0125 W m^{-2}. This indicates that, for the entire atmospheric column, calculations based on uniform distribution tend to underestimate the outgoing longwave radiative flux escaping to space.

It can be further observed that both CO_2 and CH_4 ΔRF_{TOA} exhibit clear seasonal

variations, with significantly larger negative values in spring (April–May) than in autumn (August–October). This is related to the stronger near-surface concentration gradients and more stable atmospheric stratification in the Arctic during spring, which enhance the modulation of radiative transfer by vertical structural differences. In addition, the magnitude of CO_2 ΔRF_{TOA} is significantly larger than that of CH_4, indicating that, under the same consideration of vertical structure perturbations, CO_2 exerts a stronger influence on Arctic longwave radiative fluxes.

3.3.3 Heating rate change

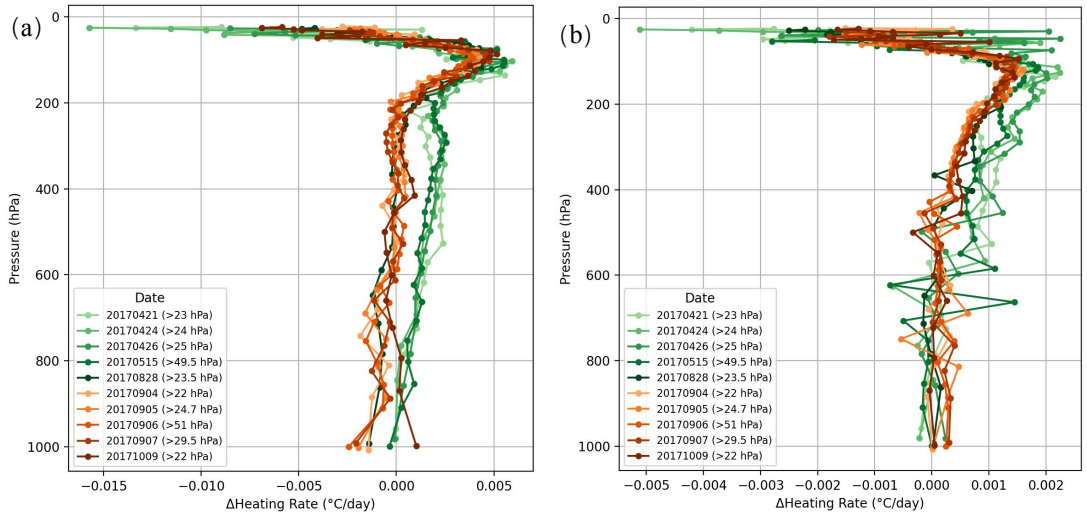

Figure.8 Vertical distribution of ΔHR associated with CO_2 (a) and CH_4 (b)

Figure 8 shows the changes in heating rates (ΔHR) for CO_2 (a) and CH_4 (b) under the uniform distribution relative to the observed vertical profiles.

As shown in Figure 8(a), the magnitude of ΔHR induced by CO_2 is mainly within $\pm$ 0.005 ° C day^{-1}, reflecting the influence of the uniform distribution assumption on the heating rate structure. In spring (April–May), ΔHR is weakly negative in the 1000–900 hPa layer, indicating that the uniform distribution assumption reduces the local heating rate near the surface relative to the observed profile.

As altitude increases to 900–200 hPa, ΔHR becomes positive and its magnitude gradually increases, indicating that the uniform distribution assumption enhances the heating rate in this layer. In the 200–100 hPa layer, ΔHR increases rapidly due to the

sharp decrease in observed CO_2 concentration relative to the uniform distribution. Above 100 hPa, ΔHR decreases again, indicating a weakening influence of the uniform distribution assumption on atmospheric heating.

In summer to autumn (August–October), ΔHR in the 1000–200 hPa layer is generally weakly negative, suggesting that the uniform distribution assumption leads to slightly weaker heating rates in the troposphere. Above 200 hPa, the vertical structure of ΔHR remains broadly consistent with that in spring.

As shown in Figure 8(b), the magnitude of ΔHR induced by CH_4 is significantly smaller than that of CO_2, mainly within ± 0.002 °C day^{-1}, indicating a relatively weaker sensitivity of longwave radiative heating to the CH_4 vertical structure. In the 1000–600 hPa layer, ΔHR is close to zero or shows slight fluctuations, suggesting that the uniform distribution assumption has only a limited influence on heating rates near the surface.

As altitude increases to 600–100 hPa, ΔHR becomes positive overall and its magnitude gradually increases. This indicates that the uniform distribution assumption enhances the heating rate in the middle and upper troposphere relative to the observed CH_4 profile. Above 100 hPa, ΔHR gradually decreases, indicating a weakening influence of the uniform distribution assumption in the upper atmosphere.

From a seasonal perspective, the overall vertical structure of CH_4 ΔHR is highly consistent between spring (April–May) and autumn (September–October), with differences mainly reflected in slight variations in the magnitude of positive heating rates in the mid-troposphere. In spring, slightly stronger positive values are observed at certain levels, possibly related to seasonal differences in atmospheric transport and vertical mixing conditions. However, these differences are relatively small and do not alter the dominant vertical structure of CH_4 ΔHR.

3.4 Layer sensitivity analysis

To further quantitatively characterize the sensitivity of TOA radiative flux to greenhouse gas perturbations at different altitudes, this study introduces the layer

radiative sensitivity kernel method to analyze the marginal radiative responses of CO_2 and CH_4 at each vertical level, thereby identifying the key altitude regions controlling radiative forcing.

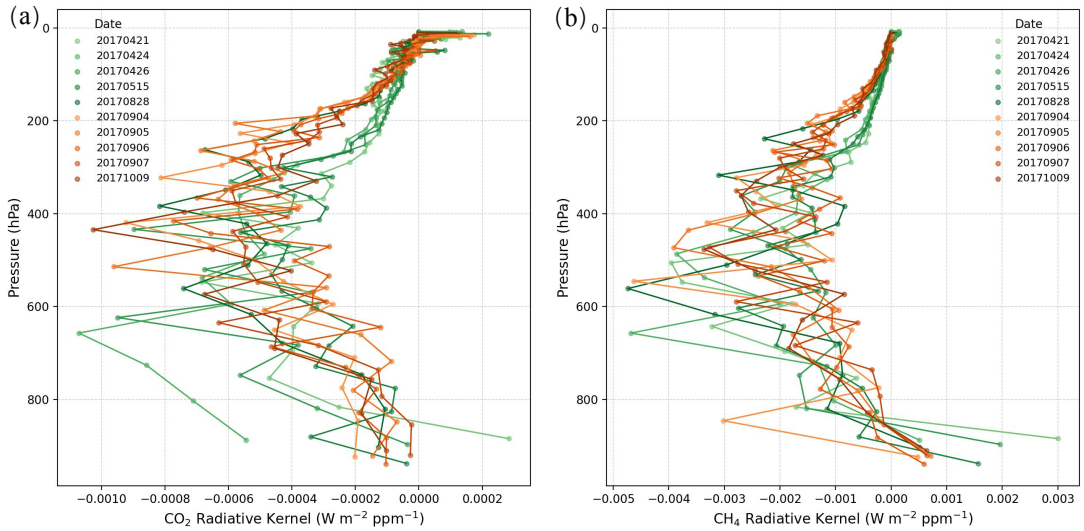

Figure.9 Vertical distributions of layer radiative kernels for CO_2 （a） and CH_4 （b） over Sodankylä

Figure 9 shows the vertical distributions of the layer radiative sensitivity kernels for CO_2 (a) and CH_4 (b) in the Arctic. In the layer radiative kernel analysis, the sign of the kernel indicates the direction of the TOA net longwave radiative flux response to a unit concentration perturbation. In this study, upward longwave radiation escaping to space at the TOA is defined as positive. When an increase in CO_2 or CH_4 concentration at a given level reduces the outgoing TOA radiation, the corresponding radiative flux change is negative, yielding a negative kernel and indicating a local heating effect. Conversely, if the concentration increase enhances outgoing TOA radiation, the kernel is positive, corresponding to a local cooling effect. It should be noted that the sign of the kernel reflects the marginal radiative response at a given level, and its contribution to the overall radiative forcing responses must be evaluated through vertical integration.

As shown in Figure 9(a), the CO_2 layer radiative sensitivity kernel exhibits a pronounced altitude dependence. The mid–upper troposphere (approximately 200–700 hPa) is the primary region contributing to the CO_2 kernel, where its absolute magnitude reaches a maximum of about 10^{-3} W m^{-2} ppm^{-1}. This indicates that, within this altitude range, an increase in CO_2 concentration significantly suppresses outgoing

longwave radiation at the TOA, corresponding to a strong local heating effect. This is mainly due to the relatively large longwave radiative flux and the unsaturated absorption of infrared radiation by CO_2 at these levels, which results in high sensitivity of TOA radiative flux to CO_2 concentration changes.

In the lower atmosphere (>700 hPa), the magnitude of the CO_2 kernel decreases significantly, indicating a weaker suppression of outgoing longwave radiation by increased CO_2 concentrations. This is primarily due to the near-saturation of infrared absorption in the lower atmosphere, as well as the presence of low-level temperature inversion in the Arctic, which further reduces the effective contribution of near-surface CO_2 increases to TOA net longwave radiative flux. In the stratosphere and above, the CO_2 kernel approaches zero, with even slightly positive values at certain levels, suggesting that under polar conditions, changes in CO_2 concentration in the upper, tenuous atmosphere have a limited impact on TOA net longwave radiation and may even slightly enhance outgoing radiation.

Overall, changes in TOA longwave radiative flux induced by CO_2 are highly sensitive to its vertical distribution. Under the same column-mean CO_2 increase, if the perturbation is concentrated in the mid–upper troposphere, it will exert a stronger suppression on outgoing TOA radiation, resulting in a stronger atmospheric heating effect.

As shown in Figure 9(b), the CH_4 layer radiative sensitivity kernel also exhibits a clear dependence on vertical structure. The maximum magnitude of the CH_4 kernel occurs in the mid-troposphere (approximately 400–700 hPa), reaching about 5×10^{-3} W m^{-2} ppm^{-1}. This indicates that, within this altitude range, an increase in CH_4 concentration significantly suppresses outgoing longwave radiation at the TOA, corresponding to a strong local heating effect. This feature is associated with the strong absorption of CH_4 in the infrared window and near-window regions, which enhances its sensitivity to TOA net longwave radiation in the relatively warm and radiatively active mid-troposphere.

With increasing altitude, the magnitude of the CH_4 kernel gradually decreases in the mid–upper troposphere, indicating that under lower temperature and weaker

radiative emission conditions, the marginal impact of CH_4 concentration increases on TOA longwave radiation becomes smaller. In the stratosphere and above, the CH_4 kernel approaches zero, suggesting that under polar background conditions, variations in CH_4 concentration in the upper atmosphere contribute little to TOA net longwave radiation, and its radiative forcing is mainly controlled by the troposphere.

Overall, the radiative forcing of CH_4 is more sensitive to the mid-troposphere, with relatively weaker dependence on the mid-upper troposphere and higher atmospheric layers. Under the same column-mean CH_4 increase, if the perturbation is primarily concentrated in the mid-troposphere, it will produce stronger radiative forcing responses at the TOA.

3.5 Chapter summary

This chapter is based on AirCore observations from the Sodankylä site in Finland and systematically analyzes the vertical distribution characteristics of CO_2 and CH_4. Combined with a radiative transfer model, it quantitatively evaluates the impact of greenhouse gas vertical structures on longwave radiative fluxes in the Arctic.

First, the observed vertical profiles of CO_2 and CH_4 are analyzed. The results show that both gases exhibit pronounced vertical inhomogeneity. CO_2 concentrations are higher in the lower troposphere during spring, whereas in late summer to autumn, near-surface concentrations are relatively lower and increase with altitude, reflecting the seasonal regulation of the Arctic carbon cycle. CH_4 maintains relatively high concentrations throughout the troposphere and decreases rapidly near the tropopause, mainly controlled by surface emissions and atmospheric chemical processes. Meanwhile, the temperature profile exhibits a typical tropospheric lapse rate and stratospheric inversion structure, and the water vapor profile shows near-surface enrichment, providing important thermodynamic and moisture background conditions for longwave radiative transfer.

On this basis, the vertical structures of net longwave radiative flux and heating rate are calculated. The results indicate that net longwave radiative flux generally

increases with altitude throughout the atmospheric column, while the heating rate remains negative at all levels, indicating that longwave radiation leads to net atmospheric radiative cooling. Radiative cooling is strongest in the lower atmosphere due to large vertical gradients in radiative flux, weakens in the mid-troposphere, and strengthens again in the upper troposphere and lower stratosphere. Seasonal variations in temperature structure and water vapor content lead to corresponding changes in the vertical distributions of radiative flux and heating rate.

Furthermore, by comparing the observed profiles with a uniform distribution scenario under the same column-mean concentrations, the radiative forcing responses induced by vertical inhomogeneity are quantitatively evaluated. The results show that the vertical structure of greenhouse gases can significantly alter the vertical distribution of radiative forcing responses within the atmospheric column. CO_2 exhibits a characteristic structure of "warming in the lower layers and cooling in the upper layers" in spring, while in autumn, as the vertical distribution becomes more uniform, the vertical gradient of its radiative forcing weakens. CH_4 shows positive radiative forcing responses throughout the troposphere and negative values in the stratosphere, reflecting its enrichment in the troposphere and rapid decrease in the stratosphere.

Both greenhouse gases produce negative TOA longwave radiative forcing responses across all observed profiles. Specifically, CO_2 ΔRF_{TOA} ranges from approximately -0.02 to -0.10 W m^{-2}, while CH_4 ΔRF_{TOA} ranges from approximately -0.01 to -0.05 W m^{-2}. This indicates that the observed vertical structure enhances outgoing longwave radiation compared with the uniform distribution, thereby strengthening radiative cooling in the Arctic atmosphere.

Finally, the layer radiative sensitivity kernel analysis further reveals the altitude-dependent sensitivity of radiative forcing. The results show that CO_2 sensitivity is mainly concentrated in the mid–upper troposphere (approximately 200–700 hPa), with a maximum value of about 10^{-3} W m^{-2} ppm^{-1}, while CH_4 exhibits peak sensitivity in the mid-troposphere (approximately 400–700 hPa), with a maximum

value close to 5×10^{-3} W m^{-2} ppm^{-1}. These results indicate that, compared with the observed vertical profiles, the use of a uniform distribution leads to an underestimation of the outgoing longwave radiative flux.

Overall, this chapter demonstrates that under Arctic conditions, the vertical distribution of greenhouse gases can significantly modulate the vertical structure of radiative forcing responses and their contribution to TOA longwave radiative flux. Therefore, when evaluating greenhouse gas radiative effects in the Arctic, it is essential to account for their vertical distribution rather than relying solely on column-mean concentrations.

4 Regional representativeness and carbon neutrality scenario analysis

4.1 Regional representativeness analysis

Based on the evaluation of greenhouse gas radiative forcing responses using single-site AirCore vertical profiles, it is necessary to further examine the representativeness of these results at larger spatial scales. Due to the complex underlying surface and the pronounced spatial heterogeneity of thermodynamic structures in the Arctic, the applicability of single-site results at the regional scale remains uncertain. Therefore, this section focuses on the selection of background atmospheric fields and systematically analyzes the stability of radiative forcing responses and the sources of their differences across different spatial scales.

Specifically, this section first evaluates the influence of different background atmospheric conditions on radiative forcing responses to verify the reliability of the single-grid background field. It then examines the variation characteristics of atmospheric thermodynamic structures across different spatial scales. On this basis, the differences in radiative forcing responses induced by greenhouse gas vertical distributions under background fields of different spatial scales are further compared, in order to comprehensively assess the representativeness of single-site results at the regional scale and their applicable spatial extent.

4.1.1 Influence of Background Atmospheric Conditions on ΔRF

Before conducting the regional representativeness analysis at different spatial scales, it is necessary to evaluate the influence of background atmospheric field selection on radiative forcing responses. Since the subsequent spatial scale comparison will use the single WACCM grid corresponding to the Sodankylä site as the reference background field, the radiative forcing responses and heating rate profiles calculated under two background conditions are first compared.

One scenario uses AirCore observations to provide both greenhouse gas concentration profiles and the corresponding atmospheric background information,

while the other keeps the greenhouse gas vertical distribution unchanged and uses background temperature and pressure from the nearest single WACCM grid to the Sodankylä site. Through this comparison, the applicability of the WACCM single-grid background field in this region can be assessed, providing a basis for subsequent spatial scale extension analyses.

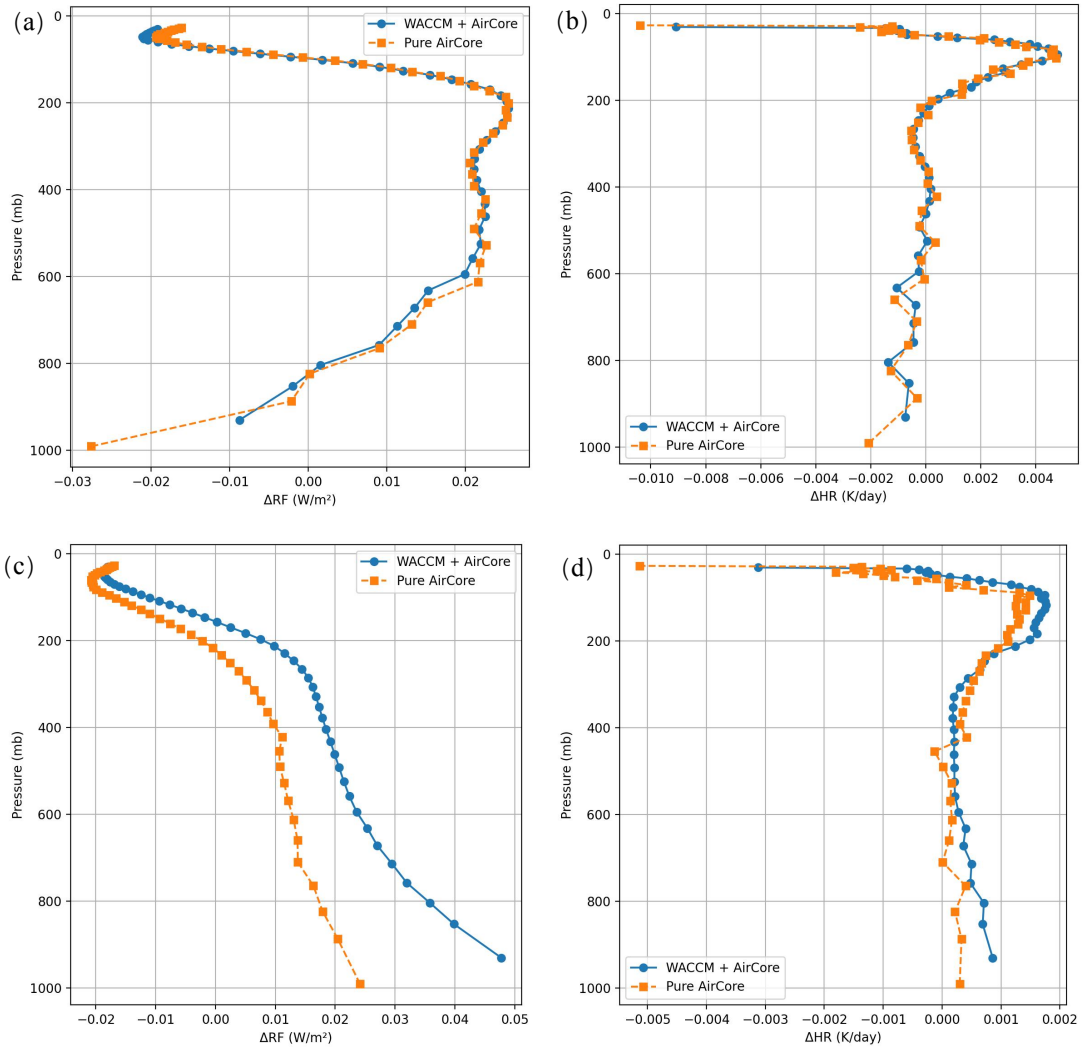

Figure.10 Comparison of Δ RF and heating rate profiles induced by the vertical distributions of CO_2 and CH_4 under different background atmospheric fields near Sodankylä. (a) RF induced by CO_2 vertical distribution using WACCM grid background with AirCore CO_2 profile and using fully AirCore-derived atmospheric profiles; (b) corresponding HR profiles for CO_2; (c) RF induced by CH_4 vertical distribution under the same experimental settings; (d) corresponding HR profiles for CH_4.

Figure 10 presents a comparison of radiative forcing responses and heating rate changes induced by the vertical inhomogeneity of CO_2 and CH_4 under two different background conditions. Figure 10(a) shows the vertical distribution of radiative forcing responses associated with the CO_2 profile as a function of pressure. The

orange curve represents results calculated using AirCore data that provide both CO_2 concentrations and the corresponding atmospheric background information, while the blue curve represents results obtained by keeping the CO_2 vertical distribution unchanged and using background atmospheric conditions (temperature and pressure) from the nearest single WACCM grid to the Sodankylä site. The radiative forcing responses under the two background conditions show high consistency in both overall structure and magnitude, with only minor differences at a few altitude levels.

The heating rate profiles shown in Figure 10(b) also exhibit good agreement, with nearly identical peak locations and vertical variation patterns, indicating that under CO_2 conditions, differences in background temperature and pressure fields have a relatively weak influence on radiative forcing responses and heating rates.

For CH_4, Figures 10(c) and 10(d) present comparisons of radiative forcing responses and heating rate changes, respectively. Compared with CO_2, CH_4 shows more noticeable differences between the two background conditions, particularly in the lower atmosphere near the surface. This is mainly related to the higher sensitivity of CH_4 absorption bands to temperature structure and water vapor distribution. However, in terms of absolute magnitude, these differences remain small and do not alter the overall vertical structure of radiative forcing responses and heating rate changes, nor do they introduce systematic structural shifts.

Overall, the four panels demonstrate that, under consistent greenhouse gas vertical distributions, the results obtained using a single-grid WACCM background field are in good agreement with those derived from AirCore-based background information in both structure and magnitude. Although CH_4 shows slightly higher sensitivity to the background field than CO_2, this difference is not sufficient to affect the overall evaluation of radiative effects. Therefore, using the single-grid WACCM background field as the reference for subsequent spatial scale comparison analyses in the Sodankylä region is reasonable and acceptable.

4.1.2 Thermodynamic Structure under Different Background Spatial Scales

Based on the confirmed applicability of the single-grid background field, the

analysis is further extended from a spatial scale perspective to examine differences in atmospheric thermodynamic structures associated with background fields of varying spatial extents. To this end, Figure 11 presents the vertical profiles of temperature under three different spatial scales of background fields.

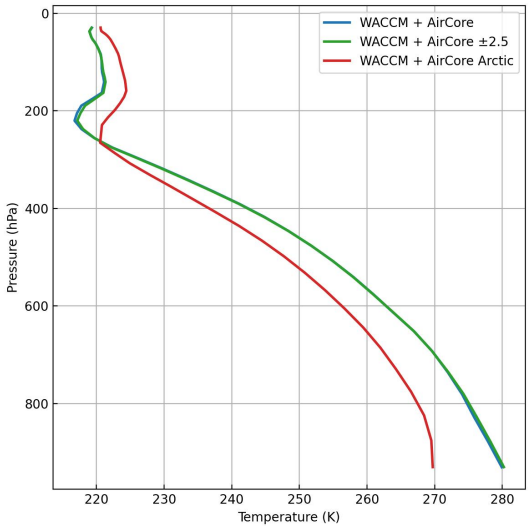

Figure.11 Vertical temperature─pressure (T─P) profiles under three background spatial scales: Sodankylä single grid, ± 2.5 ° regional mean, and Arctic mean.

Figure 11 shows the vertical temperature profiles under three different spatial scales of background fields. Overall, all three cases exhibit a typical atmospheric stratification structure: in the troposphere, temperature decreases with altitude; a clear temperature transition occurs near the tropopause; in the stratosphere, temperature increases with altitude, forming an inversion layer; and in the higher atmosphere (above approximately 100–50 hPa), temperature variations become more gradual, with a slight decreasing trend reappearing within certain altitude ranges.

Across different spatial scales, the temperature profiles from the Sodankylä single grid and the ± 2.5 ° regional mean are nearly identical, indicating strong consistency in atmospheric thermodynamic structure at the local and surrounding regional scales. In contrast, the Arctic-wide mean background field, due to its broader spatial coverage and inclusion of extensive oceanic areas, differs significantly in underlying surface properties compared to the land-dominated region around Sodankylä. This leads to systematic adjustments in the overall thermodynamic structure. As a result, the Arctic mean temperature profile exhibits a smoother vertical variation, with an overall weakened temperature gradient. In the troposphere

(approximately 1000–300 hPa), Arctic mean temperatures are generally lower than those from the single-grid and regional mean cases, while in the stratosphere (above approximately 200 hPa), they are relatively higher.

4.1.3 Spatial Scale Dependence of Radiative Forcing Profiles

Based on the thermodynamic structure differences described above, this section further analyzes the influence of background fields at different spatial scales on the radiative effects induced by greenhouse gas vertical distributions. By comparing the layer-resolved cumulative radiative forcing responses under the three background fields, the modulation of radiative processes by spatial scale variations can be quantitatively evaluated.

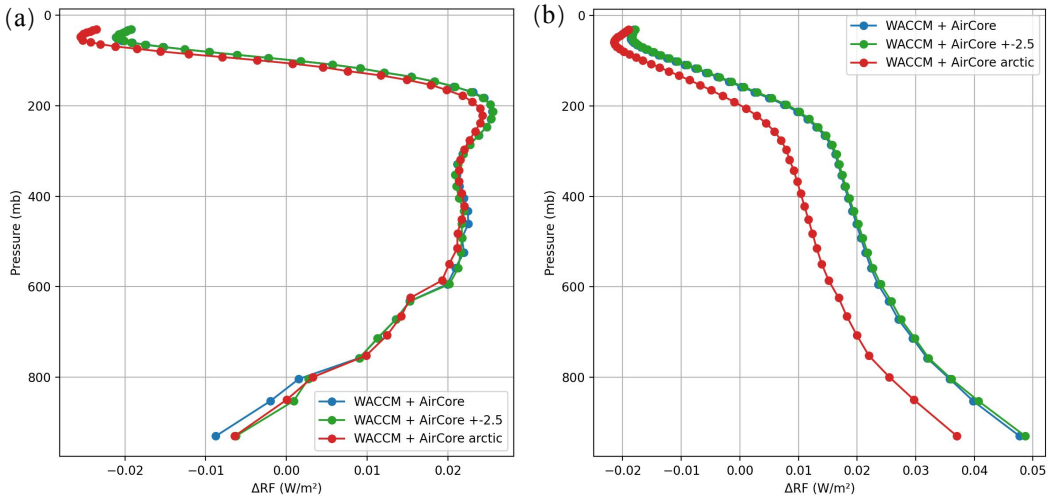

Figure.12 Vertical profiles of layer-by-layer ΔRF induced by non-uniform greenhouse gas distributions under different background spatial scales: (a) CO_2 and (b) CH_4. The three background fields include the Sodankylä single grid, the ±2.5° regional mean, and the Arctic mean.

Figure 12 presents the distributions of ΔRF induced by the vertical inhomogeneity of CO_2 (a) and CH_4 (b) under three spatial scales of WACCM background fields (Sodankylä single grid, ± 2.5 ° regional mean, and Arctic-wide mean). The blue, green, and red curves represent the results under the Sodankylä single grid, ± 2.5 ° regional mean, and Arctic-wide mean background fields, respectively.

As shown in Figure 12(a), for CO_2, the vertical structures of layer-resolved cumulative radiative forcing responses are highly consistent across the three

background fields. Although the background field becomes increasingly smoothed as the spatial scale expands from a single grid to the ± 2.5 ° regional mean and further to the Arctic-wide mean, these differences do not significantly alter the vertical structure of CO_2 radiative forcing responses. As indicated in Figure 11, the Arctic-wide mean background field is generally colder in the troposphere and relatively warmer in the stratosphere. However, due to the broad longwave absorption bands of CO_2, its effective emission heights are distributed over a wide range, and the differences in emission layer heights between the observed profile and the uniform distribution are relatively small. As a result, temperature changes exert a largely consistent influence on longwave radiative fluxes under both scenarios, leading to only minor variations in radiative forcing responses ($\Delta RF = F_{uniform} - F_{profile}$) across different background fields.

This indicates that, in the Arctic, the vertical structure of CO_2 radiative forcing responses is primarily controlled by its own concentration profile and radiative absorption characteristics, with relatively weak sensitivity to changes in the spatial scale of the background field. Therefore, expanding the spatial extent of the background field has a limited impact on the overall structure of CO_2 radiative forcing profiles.

In contrast, CH_4 exhibits a more pronounced spatial dependence under different background fields. As shown in Figure 12(b), the layer-resolved cumulative radiative forcing responses under the single-grid and ± 2.5 ° regional mean backgrounds are nearly identical, indicating that variations in thermodynamic structure at small spatial scales have a limited impact on CH_4 radiative responses when the concentration profile is fixed. However, under the Arctic-wide mean background field, the radiative forcing responses of CH_4 are systematically lower than those under the single-grid and ± 2.5 ° conditions at nearly all altitudes.

As indicated in Figure 11, this difference mainly arises from the asymmetric modulation of radiative absorption processes by lower tropospheric temperatures. In the mid–lower troposphere, CH_4 concentrations in the observed profile are higher than those in the column-mean uniform distribution, leading to stronger absorption of

longwave radiation emitted from the surface and lower atmosphere. However, under the Arctic-wide mean background field, the overall lower tropospheric temperatures reduce the upward longwave radiative flux, thereby weakening CH_4 absorption. Since the observed profile scenario is more sensitive to changes in lower-level radiative flux, the reduction in absorption is greater than in the uniform distribution scenario. This leads to a more pronounced increase in upward net radiative flux under the observed profile, ultimately resulting in a decrease in ΔRF ($F_{uniform} - F_{profile}$), manifested as a systematic negative bias.

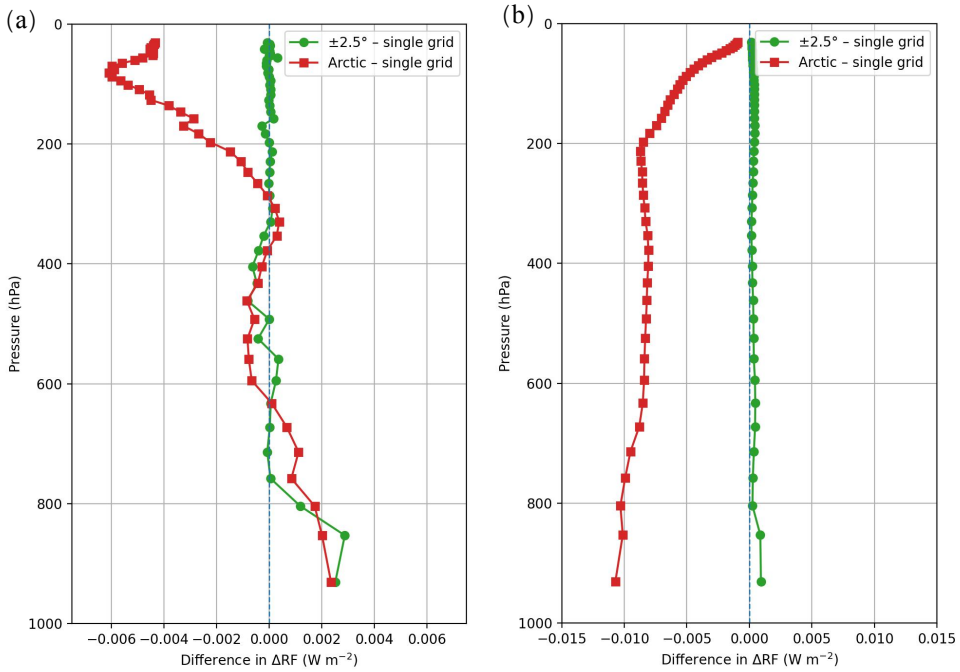

Figure.13 Vertical distribution of ΔRF relative to the single-grid reference under different background spatial scales over the Arctic region: (a) CO_2 and (b) CH_4.

Figure 13 presents the absolute differences in ΔRF for CO_2 (a) and CH_4 (b) under the ± 2.5 ° regional mean and Arctic-wide mean background fields, using the single-grid case as the reference. The green curve represents the difference between the ± 2.5 ° regional mean and the single-grid result, while the red curve represents the difference between the Arctic-wide mean and the single-grid result.

As shown in Figure 13(a), in the lower stratosphere at high latitudes (around 100 hPa), the CO_2 radiative forcing responses under the Arctic-wide mean background field are noticeably lower than those under the single-grid and ± 2.5 ° conditions, with a maximum difference of approximately −0.006 W m^{-2}. As indicated in Figure

11, temperatures at this level are relatively higher in the Arctic-wide mean background field. This change in temperature structure modulates the radiative emission processes under different concentration distributions, leading to differences in radiative forcing responses.

Specifically, in the uniform distribution scenario, the larger optical thickness shifts the effective emission layer to higher and colder altitudes, thereby weakening the enhancement of radiative flux due to increased temperature. In contrast, under the observed profile scenario, CO_2 concentrations near this level are relatively low, and the emission layer is closer to the ~100 hPa level, which is relatively warmer and more sensitive to temperature changes. As a result, the increase in net radiative flux is greater under the observed profile scenario than under the uniform distribution, leading to a further decrease in ΔRF ($F_{uniform} - F_{profile}$) and thus a more negative value. This indicates that, in the lower stratosphere, differences in radiative forcing responses are primarily governed by the coupling between effective emission height and the background temperature structure.

As shown in Figure 13(b), under the Arctic-wide mean background field, ΔRF exhibits negative values throughout the entire atmospheric column. Below 200 hPa, the difference is approximately -0.009 W m^{-2}, while above 200 hPa, the negative bias gradually decreases with altitude and approaches zero in the upper atmosphere. This vertical structure is mainly related to the altitude-dependent variations in CH_4 concentration and atmospheric density. As altitude increases, CH_4 mixing ratios decrease rapidly, leading to reduced optical thickness and a significantly weakened influence on longwave radiation. At the same time, the lower atmospheric density at high altitudes limits the magnitude of radiative flux changes induced by temperature variations. Therefore, the modulation effect of background temperature differences on the two concentration scenarios weakens with altitude, resulting in convergence of the Arctic-wide results toward the single-grid case.

In addition, since the primary absorption bands of CH_4 are concentrated in the mid–lower troposphere, its radiative responses are more directly controlled by the tropospheric temperature structure and are therefore more sensitive to large-scale

background temperature variations. This explains why, under the Arctic-wide mean background field, CH_4 ΔRF exhibits a consistent negative bias at nearly all altitudes, unlike CO_2, which shows significant differences mainly in the lower stratosphere.

4.2 Carbon neutrality scenario analysis

Under future carbon neutrality pathways, both greenhouse gas concentrations and the background atmospheric thermodynamic structure (including temperature and water vapor distributions) are expected to undergo significant changes, which may further modulate the radiative responses induced by the vertical structure of greenhouse gases. Therefore, under the SSP1-2.6 low-emission scenario, this section compares the radiative forcing responses associated with greenhouse gas vertical distributions under present-day (2017) and future (2080–2100) background conditions, with a focus on identifying the dominant mechanisms governing changes in radiative effects in the context of systematic adjustments in the climate system.

4.2.1 Atmospheric background conditions and GHG concentration settings under SSP1-2.6

Before analyzing changes in radiative forcing responses, it is first necessary to define the column-mean concentrations of greenhouse gases under different scenarios to ensure a consistent basis for comparison across background conditions.

Table.5 Column-averaged CO_2 and CH_4 concentrations used in the radiative forcing experiments for 2017 (spring and autumn) and the 2080–2100 SSP1-2.6 scenario

	2017 Spring	2017 Autumn	2080-2100
CO_2 column average concentration (ppm)	407.59	400.58	456.67
CH_4 column average concentration (ppb)	1810.8	1854.2	1121.67

Table 5 lists the column-mean CO_2 and CH_4 concentrations used in the radiative forcing calculations in this study, including observational background conditions for spring and autumn 2017, as well as the IPCC-prescribed values for the SSP1-2.6 scenario during 2080–2100.

In spring 2017, the column-mean CO_2 concentration is 407.59 ppm, while in

autumn it is 400.58 ppm, indicating a clear seasonal difference. This is related to the fact that high-latitude regions in the Northern Hemisphere have not yet entered the peak growing season in spring, and the terrestrial carbon sink has not been fully activated. In contrast, CH_4 concentrations are 1810.8 ppb in spring and 1854.2 ppb in autumn 2017, with slightly higher values in autumn, reflecting the cumulative effects of summer emissions and atmospheric transport.

For the future scenario, concentration settings are based on the SSP1-2.6 low-emission pathway from IPCC AR6. During 2080–2100, the column-mean CO_2 concentration is 456.67 ppm, which remains higher than the 2017 level, indicating that atmospheric CO_2 is still elevated even under a carbon neutrality pathway. In contrast, CH_4 concentration decreases to 1121.67 ppb, representing a substantial reduction compared to 2017 and reflecting the rapid response of methane under strong emission mitigation scenarios.

These column-mean concentrations serve as baseline values for constructing vertical profiles in subsequent analyses, providing a consistent framework for comparing radiative forcing responses induced by greenhouse gas vertical structures under present and future background conditions.

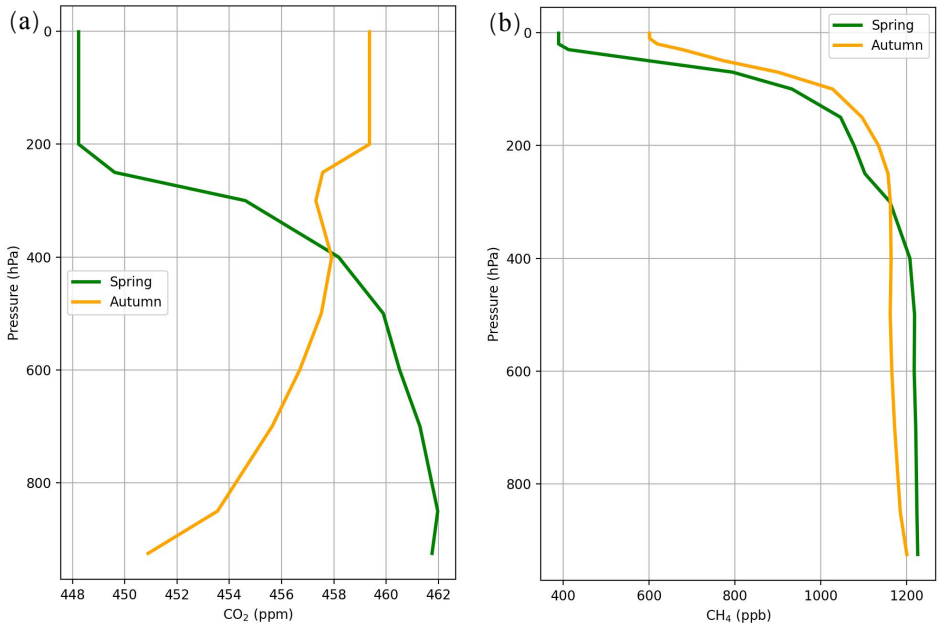

Figure.14 Vertical profiles of CO2(a) and CH4(b) used in the radiative forcing experiments for 2017 (spring and autumn) and the 2080–2100 SSP1-2.6 scenario

Figure 14 shows the vertical profiles of CO_2 and CH_4 concentrations for the

period 2080–2100 used in the radiative forcing calculations of this chapter, including both spring and autumn conditions.

For CO_2, the tropospheric profiles are constructed by proportionally scaling the 2017 AirCore observed profiles while preserving their vertical structure, according to the column-averaged concentrations given in Table 3. The stratospheric CO_2 is prescribed as a constant value equal to that at the tropopause (448.2 ppm for spring and 459.4 ppm for autumn), reflecting the significantly weakened vertical gradient under the carbon neutrality scenario.

For CH_4, the vertical profiles are obtained by uniformly scaling the 2017 AirCore observed profiles throughout the entire atmospheric column, while maintaining their original vertical structure, in accordance with the column-averaged concentrations specified in Table 3.

Since radiative transfer processes depend not only on gas concentrations but are also strongly influenced by the background atmospheric temperature structure and water vapor distribution, it is necessary to further examine the characteristics of thermodynamic structure changes under future scenarios.

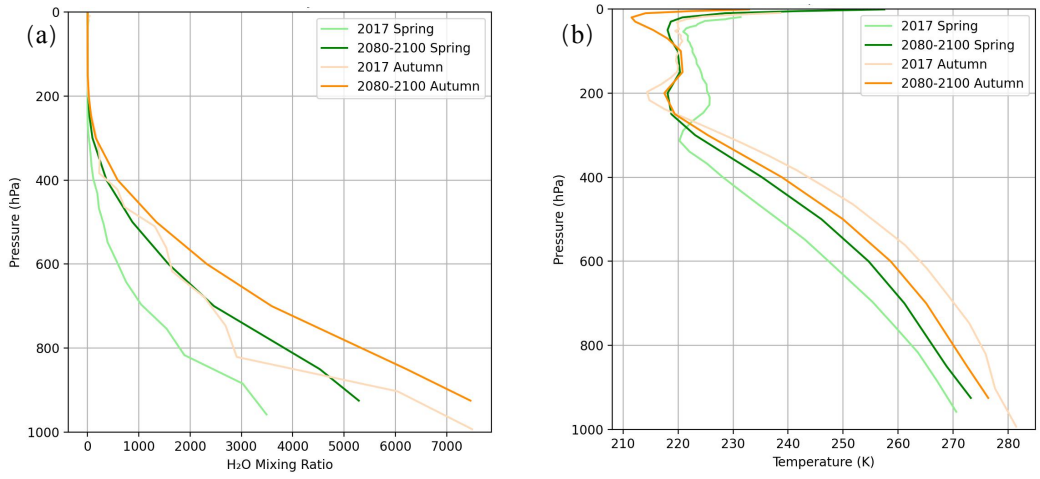

Figure.15 Vertical profiles of (a) temperature and (b) water vapor mixing ratio for spring and autumn in 2017 and 2080─2100 under the SSP1-2.6 scenario.

Figure 15 presents the vertical profiles of background atmospheric conditions for spring and autumn in 2017 and the 2080–2100 mean (SSP1-2.6 scenario), where 15(a) shows water vapor mixing ratio profiles and 15(b) shows temperature profiles.

As shown in Figure 15(a), the water vapor mixing ratio in both spring and

autumn exhibits a typical vertical structure in both periods, characterized by near-surface enrichment and a rapid decrease with altitude. Seasonally, water vapor content is consistently lower in spring than in autumn in both periods. At the same time, under the same seasonal conditions, the water vapor mixing ratio at all altitudes in 2080–2100 is significantly higher than in 2017, indicating a substantial increase in overall atmospheric humidity under future climate conditions.

As shown in Figure 15(b), the temperature profiles in both spring and autumn for 2017 and 2080–2100 exhibit a typical atmospheric stratification structure, with temperature decreasing with altitude in the troposphere and a clear inversion in the stratosphere. In spring, the mean tropospheric temperature in 2080–2100 is generally higher than in 2017, while it is slightly lower in the stratosphere. In contrast, in autumn, tropospheric temperatures in 2080–2100 are slightly lower than in 2017, while stratospheric temperatures are relatively higher. This indicates that temperature changes under future climate conditions exhibit a clear seasonal dependence and show opposite adjustment patterns across different altitude layers.

4.2.2 Radiative Forcing Responses under the SSP1-2.6 Scenario

Table.6 ΔRF_{TOA} induced by CO_2 and CH_4 vertical distribution relative to uniform mixing under 2017 and 2080─2100 (SSP1-2.6) conditions

	2017 Spring	2017 Autumn	2080-2100 Spring	2080-2100 Autumn
CO_2 ΔRF_{TOA} (W m^{-2})	-0.088	-0.014	0.004	0.009
CH_4 ΔRF_{TOA} (W m^{-2})	-0.015	-0.009	0.023	0.006

Table 6 lists the ΔRF_{TOA} induced by the vertical distributions of CO_2 and CH_4 relative to the uniform mixing assumption for spring and autumn 2017, as well as for the SSP1-2.6 scenario during 2080–2100.

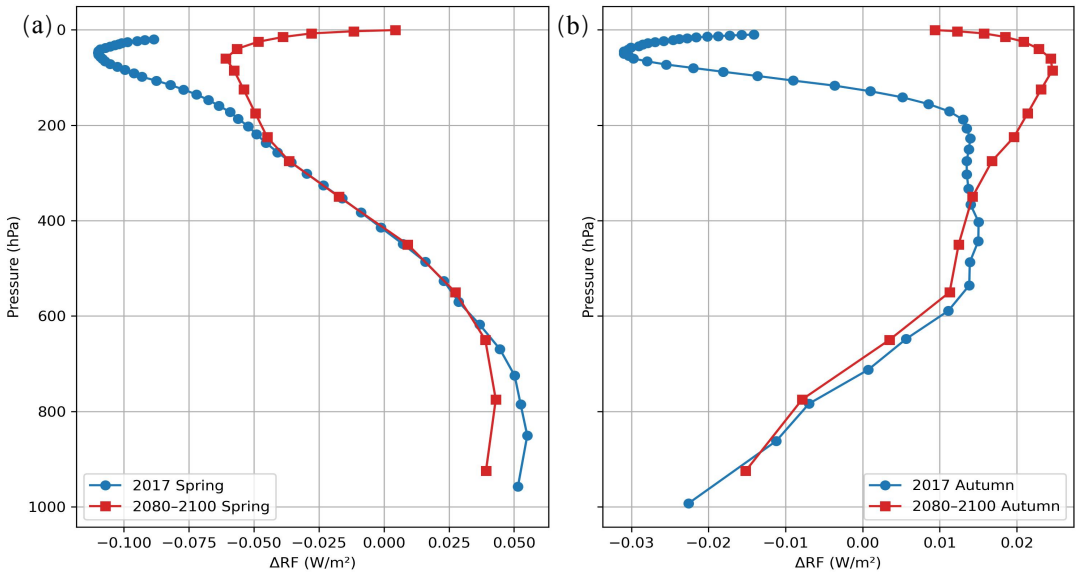

Figure.16 Vertical profiles of CO_2-induced ΔRF associated with non-uniform vertical distribution relative to uniform mixing for (a) spring and (b) autumn, comparing 2017 with 2080–2100 under the SSP1-2.6 scenario.

Figure 16 presents the vertical profiles of ΔRF induced by the CO_2 vertical distribution relative to the uniform mixing assumption. 16(a) and 16(b) represent the results for spring and autumn, respectively, and each panel compares the results for 2017 and 2080–2100 under the SSP1-2.6 scenario.

From the 2017 results, the blue profile in Figure 16(a) shows that in spring, the ΔRF induced by CO_2 vertical structure exhibits clear positive values near the surface and gradually transitions to negative values in the mid–upper troposphere, forming a pronounced stratified structure with altitude. The corresponding ΔRF_{TOA} is -0.088 W m^{-2}, indicating that the vertical structure effect in spring mainly enhances upward net radiation. In contrast, the blue profile in Figure 16(b) shows that the autumn profile differs significantly from that in spring, with weaker ΔRF near the surface and negative values at the surface. The autumn ΔRF_{TOA} (-0.014 W m^{-2}) is slightly higher than that in spring. Overall, when ΔRF_{TOA} is used as an indicator of the net radiative effect of the atmospheric column, both seasons exhibit negative values, but the magnitude of the vertical response is larger in spring, demonstrating a clear seasonal dependence of ΔRF.

Under the future SSP1-2.6 scenario, the red profile in Figure 16(a) and 16(b) show that the vertical structures of layer-resolved cumulative radiative forcing

responses in spring and autumn during 2080–2100 remain broadly consistent with those in 2017. The profiles still exhibit positive values near the surface that gradually weaken and adjust with increasing altitude, indicating that the structural influence of CO_2 vertical distribution on radiative flux remains stable.

However, both the sign and magnitude of ΔRF_{TOA} change significantly. In 2080–2100, the spring CO_2 ΔRF_{TOA} is 0.004 W $m^{-2,}$ shifting from -0.088 W m^{-2}, in spring 2017 to a positive value; in autumn, it is 0.009 W m^{-2}, also shifting from -0.014 W m^{-2}, in 2017 to a positive value. Overall, under the future scenario, the ΔRF_{TOA} induced by CO_2 vertical structure change from negative to positive, with the magnitude in spring remaining significantly larger than in autumn.

From the perspective of column-mean concentration changes, CO_2 concentrations are 407.59 ppm and 400.58 ppm in spring and autumn 2017, respectively, and increase to 456.67 ppm during 2080–2100. Correspondingly, the ΔRF_{TOA} are overall enhanced.

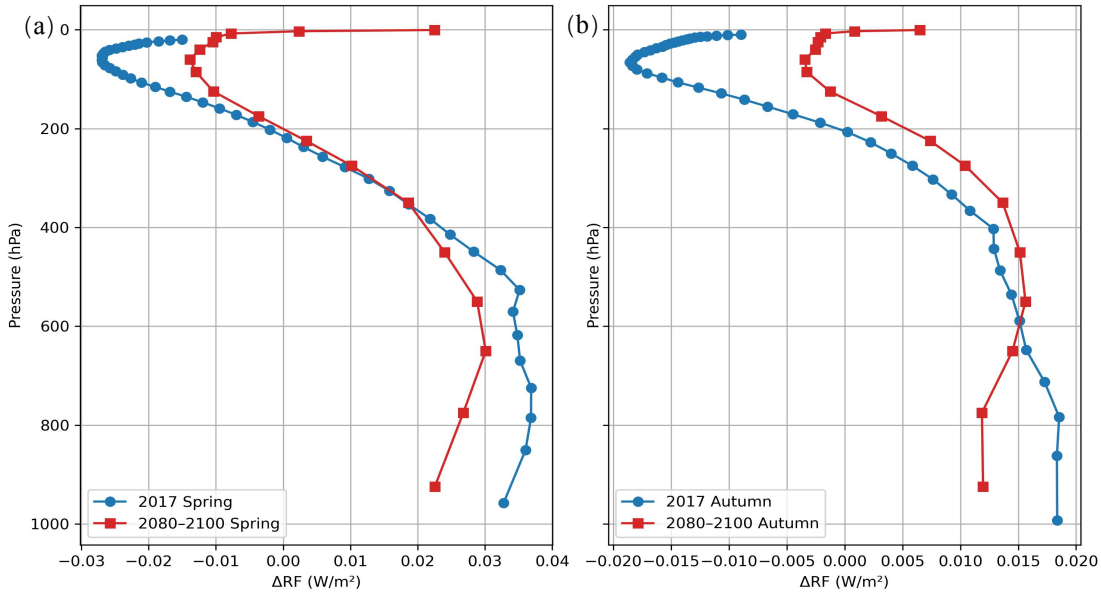

Figure.17 Vertical profiles of CH_4 -induced radiative forcing response (ΔRF) associated with non-uniform vertical distribution relative to uniform mixing for (a) spring and (b) autumn, comparing 2017 with 2080–2100 under the SSP1-2.6 scenario.

Figure 17 presents the vertical profiles of ΔRF induced by the CH_4 vertical distribution relative to the uniform mixing assumption. 17 (a) and 17(b) represent the results for spring and autumn, respectively, and each panel compares the results for 2017 and 2080–2100 under the SSP1-2.6 scenario.

Similar to CO_2, the layer-resolved cumulative radiative forcing responses of CH_4 exhibit clear structural characteristics under different scenarios. In spring and autumn 2017, positive radiative forcing dominates in the lower atmosphere, while negative adjustments appear in the upper layers (particularly from the upper troposphere to the lower stratosphere), forming a vertical structure characterized by positive in the lower layers and compensating negative aloft. This opposite-sign distribution between lower and upper layers results in a negative ΔRF_{TOA}: -0.015 W m^{-2} in spring and -0.009 W m^{-2} in autumn 2017.

Under the SSP1-2.6 scenario during 2080–2100, the vertical structure of layer-resolved cumulative radiative forcing responses remains broadly similar to that in 2017, indicating that the structural influence of CH_4 vertical distribution on radiative flux does not change significantly. However, the magnitude of the radiative forcing increases substantially, and the sign of ΔRF_{TOA} shifts from negative to positive. In 2080–2100, the CH_4 ΔRF_{TOA} is 0.023 W m^{-2} in spring and 0.006 W m^{-2} in autumn, both significantly higher than -0.015 W m^{-2} and -0.009 W m^{-2} in 2017, with the strongest response occurring in spring.

From the perspective of column-mean concentration changes, CH_4 concentrations are approximately 1810–1854 ppb in 2017 and decrease to 1121.67 ppb during 2080–2100. Despite this reduction in column-mean concentration, the ΔRF_{TOA} still increase significantly in magnitude and shift from negative to positive values.

Overall, under the SSP1-2.6 scenario, although CO_2 and CH_4 exhibit different trends in column-mean concentration changes, the ΔRF_{TOA} induced by their vertical inhomogeneity both shift from negative to positive. Compared with the observed vertical profiles, the use of a uniform distribution leads to an underestimation of the outgoing longwave radiative flux. This indicates that the changes in radiative forcing responses are not driven by concentration changes of a single gas, but rather result from the combined effects of systematic adjustments in the background atmospheric state.

First, the increase in water vapor is the most critical modulating factor.

Compared with 2017, water vapor concentrations at all altitudes are higher in both spring and autumn during 2080–2100. The increase in water vapor significantly enhances the longwave optical thickness of the atmosphere, elevating the effective radiative emission level and thereby altering the vertical control of radiative flux. Under such high optical thickness conditions, the sensitivity of outgoing longwave radiation to vertical concentration gradients of greenhouse gases is markedly enhanced. In other words, the same concentration distribution differences lead to larger differences in radiative flux responses. For the observed profile distribution, higher greenhouse gas concentrations in the lower layers more effectively enhance longwave absorption under humid conditions, resulting in a relative decrease in $F_{profile}$. In contrast, the response under the uniform distribution is weaker, leading to a substantial increase in ΔRF ($F_{uniform} - F_{profile}$) and a transition to positive values under the SSP1-2.6 scenario. Therefore, the increase in water vapor amplifies the ΔRF_{TOA} induced by vertical inhomogeneity by increasing atmospheric optical thickness and enhancing radiative sensitivity to vertical structure, making it the dominant factor driving the strengthening of structural radiative effects in the future.

Second, the combined effect of stratospheric cooling and tropospheric warming in spring further amplifies the radiative forcing responses. In spring, the stratospheric temperature in 2017 is generally higher than that under the SSP1-2.6 scenario, whereas future stratospheric cooling weakens the longwave emission capability of the upper atmosphere, thereby reducing the compensating cooling effect from aloft. Under such conditions, when greenhouse gases are vertically inhomogeneous within the troposphere, the radiative changes induced by enhanced absorption in the lower layers are less effectively offset by upper-layer emissions, making the ΔRF_{TOA} more likely to be positive. Meanwhile, tropospheric temperatures in spring are slightly higher in the future scenario, and since the observed vertical profile features higher greenhouse gas concentrations in the lower layers, the absorption of longwave radiation is further enhanced, increasing the difference in radiative flux between different distribution scenarios. Because this structural change, stratospheric cooling combined with tropospheric warming, is more pronounced in spring than in autumn,

the magnitude of the transition of the ΔRF_{TOA} from negative to positive in spring is significantly greater than that in autumn under the SSP1-2.6 scenario.

Under this background, the increase in CO_2 concentration from approximately 400–408 ppm to 456 ppm plays a secondary, modulating role. Higher CO_2 concentrations enhance the baseline absorption within its spectral bands, allowing vertical gradient-induced absorption differences to produce stronger flux responses under higher optical thickness conditions. However, this effect mainly amplifies the background radiative sensitivity rather than serving as the primary driver of structural radiative enhancement.

In contrast, although CH_4 column-mean concentration decreases in the future scenario, its ΔRF_{TOA} still shifts from negative to positive. This further demonstrates that column-mean concentration is not the controlling factor. Under the combined influence of increased humidity and temperature structure adjustments, the atmospheric radiative balance shifts, enhancing the system's sensitivity to vertical gradients and causing the TOA manifestation of CH_4 structural differences to change from negative to positive. Therefore, changes in CH_4 concentration play only a secondary role, while its radiative forcing responses are primarily modulated by background thermodynamic conditions.

Overall, this study demonstrates that the radiative forcing responses induced by vertical inhomogeneity of greenhouse gases exhibit strong background dependence. Increased humidity and stratospheric cooling constitute the dominant mechanisms driving the enhancement of structural radiative effects in the future, while changes in gas concentrations act mainly as modulators. This implies that under different climate background conditions, neglecting the vertical structure of greenhouse gases may lead to systematic biases in estimating radiative forcing in the Arctic, and such biases may become more pronounced under emission reduction scenarios.

4.3 Chapter summary

This chapter focuses on the spatial representativeness of radiative effects induced

by the vertical distribution of greenhouse gases and their variations under future climate conditions, and systematically conducts a regional representativeness and carbon neutrality scenario analysis.

In the regional representativeness analysis, the applicability of the single-grid background field in the Sodankylä region is first validated by comparing the profiles of radiative forcing responses and heating rate changes under AirCore-observed background conditions and single-grid WACCM background conditions. On this basis, differences in atmospheric thermodynamic structures across different spatial scales, including single grid, ± 2.5 ° regional average, and Arctic-wide average, are further analyzed, and their impacts on radiative forcing responses are evaluated. The results show that the CO_2 radiative forcing response profiles are highly stable across different spatial scales, with their vertical structure mainly controlled by the gas absorption characteristics and showing weak sensitivity to background field variations. In contrast, the CH_4 radiative forcing response profiles are more sensitive to changes in background thermodynamic structure, exhibiting systematically lower values under the Arctic-scale background field, indicating a stronger spatial dependence. Therefore, the radiative forcing responses derived from the Sodankylä single-station observations are representative at local to regional scales, approximately within the ± 2.5 ° range. However, when extended to the entire Arctic region, cumulative differences in background thermodynamic structure may introduce systematic biases.

In the carbon neutrality scenario analysis, by comparing radiative forcing responses under 2017 conditions and the SSP1-2.6 scenario during 2080 to 2100, it is found that although the column-mean concentrations of CO_2 and CH_4 exhibit different trends, the TOA radiative forcing responses induced by their vertical inhomogeneity both shift from negative to positive values, with a significant overall enhancement. This implies that under future conditions, the use of a uniform greenhouse gas profile may lead to an overestimation of the outgoing longwave radiative flux from the Arctic atmosphere. Further mechanism analysis shows that this change is not driven by the concentration of a single gas, but mainly results from systematic adjustments in the background atmospheric state. Among these factors, the increase in water vapor

enhances atmospheric longwave optical thickness and strengthens the system sensitivity to vertical gradients, making it the dominant driver of the enhanced structural radiative effect. Meanwhile, the combined effect of springtime stratospheric cooling and tropospheric warming further weakens radiative compensation in the upper layers and enhances absorption in the lower layers, thereby amplifying the radiative forcing responses, with a more pronounced increase in TOA responses in spring than in autumn.

Overall, the results of this chapter demonstrate that radiative forcing responses induced by the vertical inhomogeneity of greenhouse gases exhibit both spatial scale dependence and strong sensitivity to changes in climate background conditions. Under future low-emission climate scenarios, neglecting the vertical structure of greenhouse gases may lead to a systematic overestimation of outgoing longwave radiative flux in the Arctic. This finding has important implications for studies of radiative forcing responses induced by vertical inhomogeneity of greenhouse gases at regional scales and under future climate scenarios.

5 Conclusions and outlook

5.1 Main conclusion

Based on high-resolution AirCore observational profiles at the Sodankylä site in Finland in 2017, this study combines the RRTMG model and constructs comparative experiments between 'observed vertical profiles' and 'column-mean uniform distributions' to systematically investigate the impacts of vertical inhomogeneity of CO_2 and CH_4 on clear-sky instantaneous longwave radiative forcing and heating rate structures in the Arctic. Furthermore, the spatial representativeness and responses under the SSP1-2.6 carbon neutrality scenario are evaluated. The results indicate that the vertical structure of greenhouse gases is an important factor influencing the Arctic radiative budget, and its effects strongly depend on seasonal variations and background atmospheric conditions. The main conclusions of this study are as follows:

(1) The vertical structure of greenhouse gases significantly modulates longwave radiative fluxes. The layer-resolved cumulative radiative forcing responses of CO_2 exhibit a typical structure with positive values in the lower layers and negative values in the upper layers. In spring, the ΔRF_{TOA} range from -0.08 to -0.11 W m^{-2}, significantly stronger than those in autumn, which range from -0.01 to -0.04 W m^{-2}. For CH_4, positive forcing of about 0.02 to 0.04 W m^{-2} occurs in the lower and middle troposphere, while negative forcing of about -0.02 to -0.03 W m^{-2} appears in the upper layers. Overall, the ΔRF_{TOA} of both CO_2 and CH_4 are negative. These results suggest that under the current cold and dry Arctic background, the column-mean assumption underestimates the outgoing longwave radiation.

(2) Radiative forcing exhibits strong altitude dependence on the location of vertical perturbations, and different gases have distinct key sensitive layers. Layer sensitivity analysis shows that the most sensitive layer for CO_2 is located at 200 to 700 hPa, with a maximum kernel value of about 10^{-3} W m^{-2} ppm^{-1}, corresponding to a 1 ppm CO_2 perturbation. For CH_4, the most sensitive layer is located at 400 to 900 hPa, with a maximum sensitivity of about 5×10^{-3} W m^{-2} ppm^{-1}, corresponding to a 10

ppb CH_4 perturbation. This indicates that when CO_2 is concentrated in the mid to upper troposphere and CH_4 is concentrated in the mid to lower troposphere, their impacts on TOA radiative balance are most efficient. This demonstrates that the radiative effects of greenhouse gases depend not only on their total amount but also strongly on their vertical distribution.

(3) Single-station AirCore observations show good representativeness at the regional scale, while CH_4 is more sensitive to background conditions. Under different spatial-scale background fields, the differences in layer-resolved cumulative CO_2 radiative forcing responses are small, with a maximum difference of about 0.006 W m^{-2} in the 0 to 200 hPa layer. In contrast, CH_4 shows an overall reduction under the Arctic-wide background field, with a maximum difference of about 0.01 W m^{-2} near the surface, while the vertical structure remains consistent. This indicates that single-station results can represent regional-scale characteristics within a reasonable range, although CH_4 is more sensitive to variations in background thermodynamic structure.

(4) Under the SSP1-2.6 carbon neutrality scenario, the vertical structure effect remains significant, but the TOA radiative forcing responses shift from negative to positive. In the future, the column-mean CO_2 concentration increases by about 50 ppm, while CH_4 decreases by about 700 ppb, yet both ΔRF_{TOA} values change from negative to positive. At the same time, the overall layer-resolved cumulative radiative forcing responses are strengthened, suggesting that increased water vapor and changes in temperature stratification significantly enhance the atmospheric sensitivity to vertical distribution perturbations. These results indicate that under future climate conditions, the column-mean assumption will overestimates the outgoing longwave radiation.

5.2 Research innovation points

The main innovations of this study are as follows:

(1) In contrast to previous studies based on column-mean concentrations or

idealized vertical distributions, this study, for the first time, utilizes high-resolution AirCore observational profiles to quantitatively assess the impact of greenhouse gas vertical structure on instantaneous clear-sky radiative forcing in the Arctic;

(2) This effect is further extended to a carbon-neutral future scenario, revealing that under the low-emission SSP1-2.6 scenario as well, vertical inhomogeneity of greenhouse gases can still dominate the sign change of TOA radiative forcing response, highlighting its critical role in climate response assessments.

5.3 Deficiency and prospect

This study systematically analyzes the impact of greenhouse gas vertical structure on instantaneous clear-sky longwave radiative forcing in the Arctic based on AirCore observational data and RRTMG. While meaningful progress has been achieved, several limitations remain and warrant further improvement:

(1) Uncertainty due to missing boundary data in observational profiles. AirCore data exhibit partial gaps near the surface and near the top of the atmosphere. In this study, a boundary value substitution method is applied to fill these gaps, which may introduce uncertainties in radiative flux calculations in the lower and upper atmosphere. To reduce the influence of numerical instability at high altitudes, ΔRF_{TOA} is defined as the ΔRF value at the top layer after removing anomalous upper layers, which may deviate from the true TOA radiative forcing. Future work could improve profile completeness by enhancing observational techniques or integrating multi-source datasets such as satellite retrievals and radiosonde measurements, thereby reducing uncertainties in radiative calculations.

(2) Limited sample size in spatial representativeness analysis. In the spatial representativeness analysis, only one date, September 7, 2017, includes both WACCM background fields and AirCore observations. Conclusions based on a single case remain statistically limited. Future studies could expand the temporal coverage and incorporate multi-year or multi-site AirCore datasets to increase sample size and improve the robustness of spatial representativeness assessments.

(3) Low vertical resolution in future scenario simulations. In the SSP1-2.6 carbon neutrality scenario analysis, the CESM2 and CESM2-WACCM outputs used have relatively low vertical resolution, with only 18 layers. This limits the ability to accurately resolve greenhouse gas vertical structures and their radiative effects. Comparisons with high-resolution profiles from 2017 may therefore introduce uncertainties. Future work could adopt higher vertical resolution model outputs or reconstruct fine-resolution profiles through vertical interpolation to improve the accuracy of radiative forcing calculations.

(4) Neglect of cloud radiative effects and rapid adjustment processes. This study focuses on clear-sky instantaneous radiative forcing and does not account for cloud radiative effects or atmospheric rapid adjustments such as temperature, water vapor, and cloud feedbacks. In reality, clouds play a critical role in modulating longwave radiation and may alter the manifestation of vertical structure effects. Future research could extend the analysis to all-sky conditions and adopt the effective radiative forcing framework to comprehensively evaluate the overall impact of greenhouse gas vertical structure on the climate system.

(5) Idealized treatment of vertical structure in the future scenario. In the carbon-neutral scenario experiment, vertical distributions of greenhouse gases are constructed based on the 2017 AirCore profiles and scaled proportionally to match the column-mean concentrations under the SSP1-2.6 scenario, with CH_4 retaining its original structure, while CO_2 is scaled in the troposphere and prescribed as a constant in the stratosphere. This treatment assumes that the vertical structure remains largely unchanged in the future and does not account for the effects of changes in atmospheric circulation and biogeochemical processes. Future studies could incorporate model outputs or retrieval data to construct more realistic vertical distributions and improve the reliability of the results.

Reference

[1] IPCC. Climate Change 2021: The Physical Science Basis[M]. Cambridge: Cambridge University Press, 2021.

[2] IPCC. Climate Change 2023: Synthesis Report[R]. Geneva: Intergovernmental Panel on Climate Change, 2023.

[3] Kramer R J, He H, Soden B J, et al. Observational evidence of increasing global radiative forcing[J]. Geophysical Research Letters, 2021, 48(7): e2020GL091585. DOI:10.1029/2020GL091585.

[4] Quaas J, Jia H, Smith C, et al. Robust evidence for reversal of the trend in aerosol effective climate forcing[J]. Atmospheric Chemistry and Physics, 2022, 22(18): 12221 − 12239. DOI:10.5194/acp-22-12221-2022.

[5] Myhre G, Shindell D, Bréon F M, et al. Anthropogenic and natural radiative forcing[M]//Stocker T F, Qin D, Plattner G K, et al. Climate Change 2013: The Physical Science Basis. Cambridge: Cambridge University Press, 2013: 659 − 740.

[6] Etminan M, Myhre G, Highwood E J, et al. Radiative forcing of carbon dioxide, methane, and nitrous oxide: A significant revision of the methane radiative forcing[J]. Geophysical Research Letters, 2016, 43(24): 12614 − 12623. DOI:10.1002/2016GL071930.

[7] Mlawer E J, Taubman S J, Brown P D, et al. Radiative transfer for inhomogeneous atmospheres: RRTM, a validated correlated-k model for the longwave[J]. Journal of Geophysical Research, 1997, 102(D14): 16663 − 16682. DOI:10.1029/97JD00237.

[8] Iacono M J, Delamere J S, Mlawer E J, et al. Radiative forcing by long-lived greenhouse gases: Calculations with the AER radiative transfer models[J]. Journal of Geophysical Research: Atmospheres, 2008, 113: D13103. DOI:10.1029/2008JD009944.

[9] Chen Y T, Huang Y, Merlis T M, et al. The global patterns of instantaneous CO_2 forcing at the top of the atmosphere and the surface[J]. Journal of Climate, 2023,

36(17): 5643 − 5658. DOI:10.1175/JCLI-D-22-0603.1.

[10] Chen Y T, Merlis T M, Huang Y, et al. The cause of negative CO_2 forcing at the top of atmosphere: The role of stratospheric versus tropospheric temperature inversions[J]. Geophysical Research Letters, 2024, 51(3): e2023GL106725. DOI:10.1029/2023GL106725.

[11] Sweeney C, Chatterjee A, Wolter S, et al. Using atmospheric trace gas vertical profiles to evaluate model fluxes: A case study of Arctic-CAP observations and GEOS simulations for the ABoVE domain[J]. Atmospheric Chemistry and Physics, 2022, 22(9): 6347 − 6364. DOI:10.5194/acp-22-6347-2022.

[12] Karppinen T, Lamminpää O, Tukiainen S, et al. Vertical distribution of Arctic methane in 2009 − 2018 using ground-based remote sensing[J]. Remote Sensing, 2020, 12(6): 917. DOI:10.3390/rs12060917.

[13] Freckleton R S, Highwood E J, Shine K P, et al. Greenhouse gas radiative forcing: Effects of averaging and inhomogeneities in trace gas distribution[J]. Quarterly Journal of the Royal Meteorological Society, 1998, 124(548): 2099 − 2127. DOI:10.1002/qj.49712455014.

[14] Maycock A C, Smith C J, Rap A, et al. On the structure of instantaneous radiative forcing kernels for greenhouse gases[J]. Journal of the Atmospheric Sciences, 2021, 78(3): 845 − 866. DOI:10.1175/JAS-D-19-0267.1.

[15] Pincus R, Buehler S A, Brath M, et al. Benchmark calculations of radiative forcing by greenhouse gases[J]. Journal of Geophysical Research: Atmospheres, 2020, 125(23): e2020JD033483. DOI:10.1029/2020JD033483.

[16] Bellouin N, Quaas J, Gryspeerdt E, et al. Bounding global aerosol radiative forcing of climate change[J]. Reviews of Geophysics, 2020, 58(1): e2019RG000660. DOI:10.1029/2019RG000660.

[17] Huang X. Aerosol as a critical factor causing forecast biases of air temperature in global numerical weather prediction models[J]. Science Bulletin, 2021, 66(22): 2306 − 2309. DOI:10.1016/j.scib.2021.08.005.

[18] Parazoo N C, Commane R, Wofsy S C, et al. Detecting regional patterns of CO_2 fluxes with atmospheric data[J]. Proceedings of the National Academy of

Sciences of the United States of America, 2016, 113(25): 7732 − 7737. DOI:10.1073/pnas.1518945113.

[19] Notholt J, Schmithüsen H, Buschmann M, et al. Infrared radiative effects of increasing CO_2 and CH_4 on the atmosphere in Antarctica compared to the Arctic[J]. Geophysical Research Letters, 2024, 51(4): e2023GL105600. DOI:10.1029/2023GL105600.

[20] Nazarenko L, Xie S C, Huang J, et al. Future climate change under SSP emission scenarios with GISS-E2.1[J]. Journal of Advances in Modeling Earth Systems, 2022, 14(3): e2021MS002871. DOI:10.1029/2021MS002871.

[21] Meinshausen M, Raper S C B, Wigley T M L. The shared socio-economic pathway (SSP) greenhouse gas concentrations and their extensions to 2500[J]. Geoscientific Model Development, 2020, 13(15): 3571 − 3605. DOI:10.5194/gmd-13-3571-2020.

[22] Farago E Z, McBride L A, Hope A P, et al. AR6 updates to RF by GHGs and aerosols lowers the probability of accomplishing the Paris Agreement compared to AR5 formulations[J]. Earth System Dynamics, 2025, 16(5): 1739 − 1758. DOI:10.5194/esd-16-1739-2025.

[23] Marsh D R, Mills M J, Kinnison D E, et al. Climate change from 1850 to 2005 simulated in CESM1(WACCM)[J]. Journal of Climate, 2013, 26(19): 7372 − 7391.

[24] Liu H L, Bardeen C G, Foster B T, et al. Development and validation of the Whole Atmosphere Community Climate Model with thermosphere and ionosphere extension (WACCM-X 2.0)[J]. Journal of Advances in Modeling Earth Systems, 2018, 10(2): 381 − 402.

[25] Shams S B, Walden V P, Petropavlovskikh I, et al. Variations in the vertical profile of ozone at four high-latitude Arctic sites from 2005 to 2017[J]. Atmospheric Chemistry and Physics, 2019, 19: 9733-9751. DOI:10.5194/acp-19-9733-2019.

[26] Soden B J, Held I M, Colman R, et al. Quantifying climate feedbacks using

radiative kernels[J]. Journal of Climate, 2008, 21(14): 3504 − 3520. DOI:10.1175/2007JCLI2110.1.

[27] Huang H, Huang Y, Chen X, et al. Radiative sensitivity quantified by ERA5 kernels[J]. Earth System Science Data, 2023, 15: 3001 − 3024. DOI:10.5194/essd-15-3001-2023.

Acknowledgements

As this thesis comes to a close, I would like to take a moment to express my sincere gratitude to those who have supported me along the way.

I am especially grateful to my supervisor, Prof. Jianning Sun and Prof. Huilin Chen, for their patient guidance and unwavering support throughout every stage of this work, from the initial formulation of the research topic to the final completion of the thesis. Under their mentorship, I have gradually developed my research skills and gained a clearer understanding of the field. Their guidance has also had a positive influence on my academic and personal growth. I also wish to thank Prof. Yi Huang and Dr. Ruogu He for their valuable advice in refining the research direction and for their guidance in the application of radiative transfer models. And I would like to thank Prof. Ivan Mammarella for reviewing this thesis and for her valuable comments.

I would like to extend my appreciation to all members of the Carbon Cycle and Greenhouse Gas Research Group for their collegiality, support, and the collaborative spirit that made this journey both productive and enjoyable. I am equally thankful to my fellow students at Nanjing-Helsinki Institute in Atmospheric and Earth System Sciences, with whom I shared not only academic work, course projects and presentations, but also many memorable moments outside the classroom, including meals, outings, and various activities that enriched my graduate experience.

My deepest gratitude goes to my family, my parents and grandparents, for their unconditional love, understanding, and constant support in all my choices.

After two years of growth and change, I hope to move forward with both determination and a sense of freedom.